THEORY OF SUPERCOOLED LIQUIDS AND GLASSES: ENERGY LANDSCAPE AND STATISTICAL GEOMETRY PERSPECTIVES

Pablo G. Debenedetti,* Thomas M. Truskett, and Catherine P. Lewis

Department of Chemical Engineering, Princeton University, Princeton New Jersey 08544

Frank H. Stillinger

Bell Laboratories, Lucent Technologies, Murray Hill, New Jersey 07974 and Princeton Materials Institute, Princeton, New Jersey 08544

The glassy state is ubiquitous in nature and technology. The most common way of making a glass is by cooling a liquid sufficiently fast so that it does not have time to crystallize. The manner in which such supercooled liquids acquire amorphous rigidity is poorly understood. This lack of knowledge impacts negatively on the design, formulation, and manufacturing of important products in the pharmaceutical,

* Corresponding author (E-mail: pdebene@princeton.edu).

ADVANCES IN CHEMICAL ENGINEERING, VOL. 28
0065-2377/01 $35.00

food, communications, energy, and engineering plastics industries. We review important recent advances in the fundamental understanding of glasses that have resulted from two complementary statistical mechanical viewpoints: the energy landscape formalism and statistical geometry. The former provides a unifying analytical framework for describing the thermodynamic and transport properties of glasses and the viscous liquids from which they are commonly formed. Statistical geometry addresses the quantitative description of a glassy material's history-dependent structure.

I. Introduction

Glasses are disordered solids. At the molecular level, they have a liquid-like structure and therefore lack the periodicity of crystals. Mechanically, they behave like solids, since they exhibit proportionality between stress and deformation under moderate perturbation. Glasses have played a central role in our daily lives since ancient times. Man-made glass objects, now almost 5000 years old, have been found in Egypt (Zarzycki, 1991). Ordinary window glass, made mostly of sand (SiO_2), lime ($CaCO_3$), and soda (Na_2CO_3), is the best-known example of a manufactured amorphous solid. The superior properties of pure SiO_2 sometimes justify the substantial additional costs associated with its purification and high melting point, 1713°C (Angell and Kanno, 1976). Optical wave guides, for example, consist of pure glassy silica. Most engineering plastics are amorphous, as is the silicon used in many photovoltaic cells. In the pharmaceutical industry, glasses made of sugars and small amounts of water are commonly used for the preservation of vaccines and labile biochemicals (Franks, 1994). Metallic glasses (Chaudhari and Turnbull, 1978) command technological interest because of their soft magnetism and, in the case of some alloys, their excellent corrosion resistance (Greer, 1995). The glassy state is also important in the manufacture and processing of cookies, crackers, and other cereal-based foods (Blanshard and Lillford, 1993).

In spite of the ubiquity and technological importance of the vitreous state, the literature of our profession is quite thin on the subject. In part this is because many of the important technical problems that chemical engineers have so successfully solved in the past have been closely related to the petroleum industry and, hence, involve primarily physical and chemical transformations that take place in fluids. Glasses, moreover, being structurally liquid-like but mechanically solid, and having history-dependent properties that nevertheless can persist unchanged over geological times, fall

between the clear-cut boundaries into which chemical engineering science has traditionally been divided. The properties of a glass, for example, are as much a consequence of thermodynamics as they are of kinetics. The former provides the driving force toward equilibrium, the attainment of which is thwarted by following a path- and rate-dependent process that leads to the glassy state. This interplay of kinetics and thermodynamics, then, endows a glass with its physical properties. Like any nonequilibrium material, a glass has a processing history-dependent structure, another concept the quantification of which chemical engineering, with its traditional emphasis in fluid-phase transformations, has not been much concerned with in the past.

These reasons for the comparative marginality of glass science within the chemical engineering literature are rapidly becoming obsolete. Important industries that until recently had received comparatively little attention have become central to the theory and practice of modern chemical engineering. The pharmaceutical industry is perhaps the best example of this evolution. This situation represents a useful broadening of our discipline's scope, complementary rather than antithetical to its traditional petrochemical core. For chemical engineers involved in such activities as the design and synthesis of new materials, the formulation of pharmaceutical products, or the processing of cookies and crackers, knowledge of the solid states of matter is essential. We believe that the evolving needs of our practical profession, coupled with the trend in virtually all areas of contemporary scholarship toward a lowering of barriers between traditional disciplines will bring the vitreous state closer to the core of chemical engineering. This will enrich our discipline and should in turn lead to novel insights that will improve our basic understanding of the vitreous state of matter.

In this article we review important recent advances in the fundamental understanding of glasses that have resulted from two complementary statistical mechanical viewpoints: statistical geometry and the energy landscape. The former addresses the quantitative description of structure. The latter provides a unifying framework for describing both the thermodynamic and transport properties of glasses and the viscous liquids from which they are commonly formed. There are several excellent reviews of this vast topic. Kauzmann's (1948) classic article remains timely today and is still one of the best introductions to the field. More recent reviews include the articles by Angell (1995), Ediger *et al.* (1996), and Angell *et al.* (2000).

A. Phenomenology of Vitrification by Supercooling

Glasses can be made by a variety of processes, such as reactive precipitation, electrolytic deposition, quenching of a vapor, ion implantation,

chemical vapor deposition, and cold compression of crystals (Zarzycki, 1991; Angell, 1995; Debenedetti, 1996). The most common route to the glassy state, however, is the rapid cooling of a melt. Thus, the properties of metastable liquids cooled below their freezing point (supercooled liquids) are intimately related to those of the resulting glass.

Substances known to form glasses include elements (e.g., P, S, Se); oxides (e.g., SiO_2, GeO_2, B_2O_3, P_2O_5, As_2O_3, Sb_2O_3); chalcogenides (e.g., As_2S_3); halides (e.g., BeF_2, $ZnCl_2$); salts (e.g., $KNO_3 + Ca(NO_3)_2$, $K_2CO_3 + MgCO_3$); aqueous solutions of salts, acids, or bases [e.g., H_2SO_4 (aq.), LiCl (aq.)]; organic compounds (e.g., glycerol, methanol, ethanol, glucose, *o*-terphenyl, fructose); polymers [e.g., polystyrene, poly(vinyl chloride), poly(ethylene oxide)]; metal alloys (e.g., Ni + Nb, Cu + Zn); and metal–metalloid alloys (e.g., Pd + Si, Ni + P) (Zarzycki, 1991; Debenedetti, 1996). A glass can be formed provided that the starting liquid is cooled fast enough to avoid crystallization. The cooling rate needed to achieve this is substance-specific. Phenyl salicylate, for example, vitrifies when cooled at a rate of 50°C/s, whereas the vitrification of Ag requires cooling at 10^{10} °C/s (Uhlmann, 1972). In general, high entropies of fusion and high interfacial tensions favor vitrification (Debenedetti, 1996).

Figure 1 (Debenedetti, 1996) illustrates the relationship between the specific volume and the temperature of a liquid as it is rapidly cooled at a constant pressure. As the temperature is lowered below the freezing point T_m, the liquid contracts (provided that its thermal expansion coefficient is positive). Cooling causes molecular motion, and hence configurational exploration, to slow down. Eventually, a condition is reached where molecules move so slowly that the liquid cannot equilibrate in the available time imposed by the cooling rate, and its structure appears "frozen" on the laboratory time scale (e.g., minutes). This falling-out of equilibrium occurs across a narrow transformation range where the thermal expansion coefficient decreases abruptly to a value generally smaller than that corresponding to the liquid and comparable to that of a crystalline solid. The resulting material is a glass. The temperature defined by the intersection of the liquid and vitreous portions of the volume-vs-temperature curve is the glass transition temperature T_g. Other thermodynamic properties behave analogously to the volume, as illustrated in Fig. 2 for the enthalpy (Debenedetti, 1996).

In contrast to the freezing point, T_g is not a true transition temperature, because the vitrification process occurs over a narrow temperature interval. Furthermore, T_g depends on the cooling rate. The slower a liquid is cooled, the longer the time available for configurational exploration, and hence the lower the temperature down to which the liquid can remain in equilibrium. Consequently, T_g increases with cooling rate (Moynihan *et al.*, 1976; Brüning and Samwer, 1992). This means that the properties of a glass depend on the

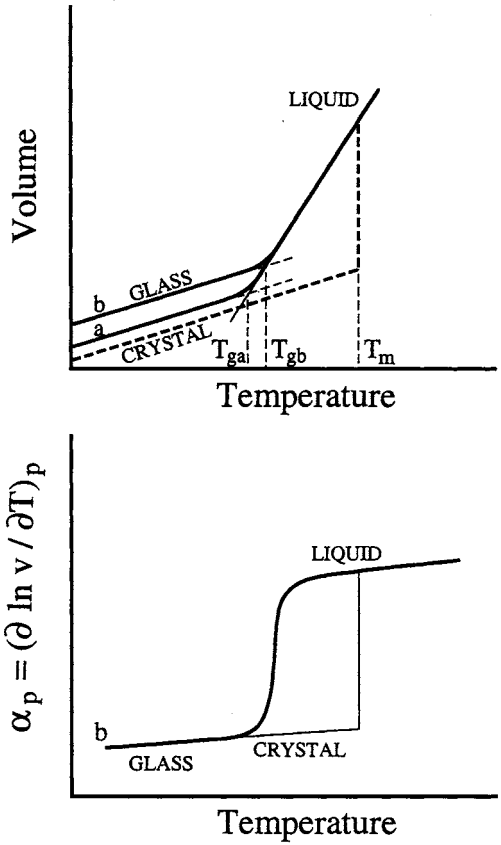

FIG. 1. Isobaric relationship between volume and temperature in the liquid, glassy, and crystalline states. T_m is the melting temperature, and T_{ga} and T_{gb} are the glass transition temperatures corresponding to slow (a) and fast (b) cooling rates. The lower diagram shows the behavior of the thermal expansion coefficient corresponding to curve b. (From Debenedetti, 1996.)

process by which it is formed. The material formed by cooling at a slower rate (Fig. 1, a), is denser and has a lower enthalpy than the faster-cooled glass, b. In practice, however, the dependence of T_g on the cooling rate is rather weak [T_g changes by only 3–5°C when the cooling rate changes by an order of magnitude (Ediger *et al.*, 1996)], and the transformation range is sufficiently narrow, so that T_g is indeed an important material characteristic (Debenedetti, 1996).

The narrow transformation range commonly referred to as *the glass transition* is the temperature interval where the characteristic molecular relaxation time becomes of the order of 100 s (the laboratory time scale). The viscosities of several glass-forming liquids are shown in Fig. 3 as a

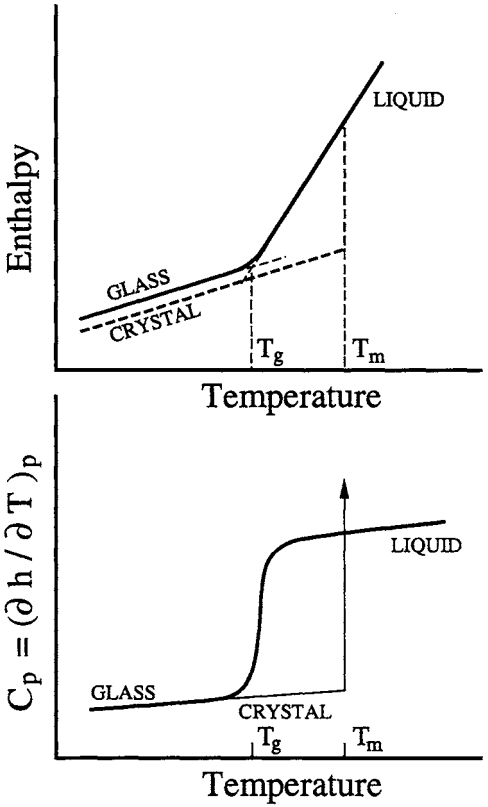

FIG. 2. Isobaric relationship between enthalpy and temperature in the liquid, glassy, and crystalline states. T_m is the melting temperature, and T_g the glass transition temperature. The lower diagram shows the behavior of the isobaric heat capacity. The arrow indicates the δ-function singularity due to latent heat at a first-order phase transition. (From Debenedetti, 1996.)

function of the reciprocal temperature. Another common definition of T_g is the temperature at which $\eta = 10^{13}$ P. Close to the glass transition the viscosity is extraordinarily sensitive to temperature. For some melts, such as silica, this dependence is well described by the Arrhenius functionality, $\eta = A \exp(E/kT)$. Other substances exhibit an even more dramatic increase in their viscosity close to the glass transition, which is often well represented by the Vogel–Tammann–Fulcher (VTF) equation (Vogel, 1921; Tammann and Hesse, 1926; Fulcher, 1925)

$$\eta = A \exp[B/(T - T_0)], \tag{1}$$

where $T_g > T_0 > 0$. Understanding the origin of this extraordinary

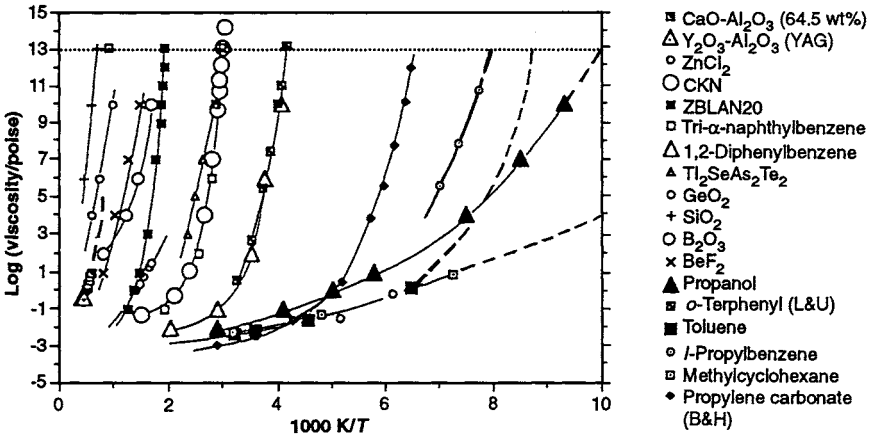

FIG. 3. Arrhenius plot of the viscosity of several supercooled liquids. The horizontal dotted line, where the viscosity reaches 10^{13} P, is commonly used as a definition of the glass transition. (Reprinted with permission from C. A. Angell. Formation of glasses from liquids and polymers. *Science* (1995); 267:1924. Copyright © (1995), American Association for the advancement of Science.)

slowing-down of molecular relaxation processes, or, equivalently, of the energy barriers that give rise to Arrhenius (or super-Arrhenius) behavior, is one of the major challenges in the physics of glasses.

Following an idea proposed by Laughlin and Uhlmann (1972), Angell (1985) plotted the viscosity of several glass-forming liquids in Arrhenius fashion but with the reciprocal temperature scaled by T_g (see Fig. 4). Since all curves coincide at T_g (where $\eta = 10^{13}$ P), and at high temperatures, where η is close to 10^{-2} P for many liquids above their melting point (e.g., water), a more orderly pattern emerges from this scaled Arrhenius representation, compared to the bare Arrhenius plot shown in Fig. 3. Angell proposed a useful classification of liquids into "strong" and "fragile" categories. The viscosity of the former behaves in nearly Arrhenius fashion, whereas fragile liquids show marked deviations from Arrhenius behavior. Silica is often mentioned as the prototypical strong liquid, whereas *o*-terphenyl is the canonical fragile glass-former. In general, strong liquids, such as the network oxides SiO_2 and GeO_2, have tetrahedrally coordinated structures, whereas the molecules of fragile liquids experience nondirectional, dispersive forces. The strong–fragile pattern is not limited to the viscosity. Any molecular relaxation time,[1] when plotted in scaled Arrhenius fashion, will result in a plot similar to Fig. 4 (Angell, 1995).

[1] The viscosity is the product of the elastic modulus, G_∞, and the shear relaxation time τ, $\eta = G_\infty \tau$.

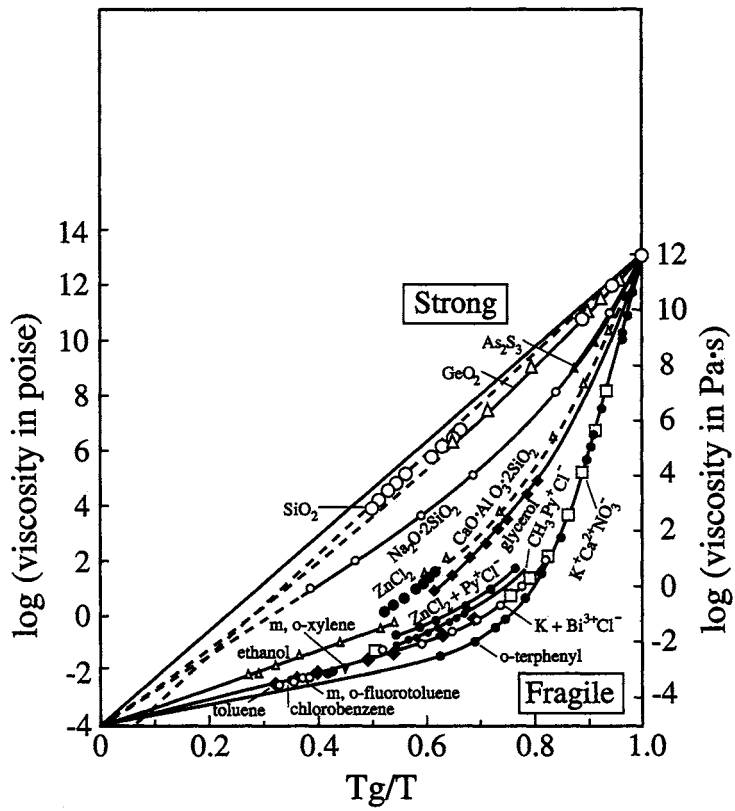

FIG. 4. The strong–fragile classification of liquids. This Arrhenius plot differs from Fig. 3 in that the temperature is scaled with T_g. Strong liquids display Arrhenius behavior; fragile liquids do not. (From Angell, 1988.)

Another important characteristic of viscous liquids close to T_g is nonexponential relaxation. Consider the response of a system to a perturbation, such as the polarization in response to an applied electric field, the strain (deformation) resulting from an applied stress, the stress in response to an imposed deformation, the volume response to applied pressure, or the temperature response to a heat flux. It is found experimentally that the temporal behavior of the response function $\Phi(t)$, following an initial "instantaneous" response, can often be described by the stretched exponential, or Kohlrausch–Williams–Watts (KWW) function (Kohlrausch, 1854; Williams and Watts, 1970),

$$\Phi(t) = \exp\{-(t/\tau)^{\beta}\} \qquad (\beta < 1), \tag{2}$$

where

$$\Phi(t) = [\sigma(t) - \sigma(\infty)]/[\sigma(0^+) - \sigma(\infty)] \tag{3}$$

and σ is the measured quantity (e.g., the instantaneous stress following a step change in deformation.) τ in Eq. (2) is a characteristic relaxation time, whose temperature dependence is often non-Arrhenius (fragile behavior.) Other functional forms, such as power-law relaxation (Richert and Blumen, 1994), have also been used to fit nonsimple exponential behavior. More important than the exact functional form (especially since those used so far are not theoretically based but empirical fits) is the considerable slowing-down of long-time relaxation embodied in KWW-type behavior. This contrasts sharply with the behavior of liquids above the melting point, which is usually well characterized by simple exponential (Debye) relaxation ($\beta \to 1$). The molecular basis of nonsimple exponential relaxation is not fully understood, but the available evidence suggests that this sluggishness is the consequence of the growth of distinct individually relaxing domains (spatial heterogeneity) (Hyde *et al.*, 1990; Richert, 1994; Cicerone and Ediger, 1995, 1996; Mel'cuk *et al.*, 1995; Hurley and Harrowell, 1996; Perera and Harrowell, 1996a,b; Donati *et al.*, 1999a; Bennemann *et al.*, 1999; Wang and Ediger, 1999; Ediger, 2000). Whether or not the individual relaxation in each of these domains is exponential is an important and interesting open question (Vidal Russell and Israeloff, 2000).

B. Open Questions

The entropy of a liquid at its melting temperature is higher than that of the corresponding crystal.[2] However, the heat capacity of a liquid is generally higher than that of the crystal. Thus, the entropy difference between a liquid and its stable crystal decreases upon supercooling. Figure 5 (Kauzmann, 1948) shows the entropy difference between several supercooled liquids and their stable crystals as a function of temperature, at atmospheric pressure. For lactic acid the entropy difference decreases so fast that a modest extrapolation of experimental data predicts its vanishing. In practice, the glass transition intervenes, and the crossing does not occur. This is shown by the dotted horizontal lines in Fig. 5. If the glass transition did not intervene, the liquid entropy would equal the crystal's at a temperature T_K (the Kauzmann temperature.) Below T_K the entropy of the crystal approaches zero as T tends to zero, and hence the entropy of the liquid would become negative

[2] See Greer (2000) and Rastogi *et al.* (1999) for an apparent exception.

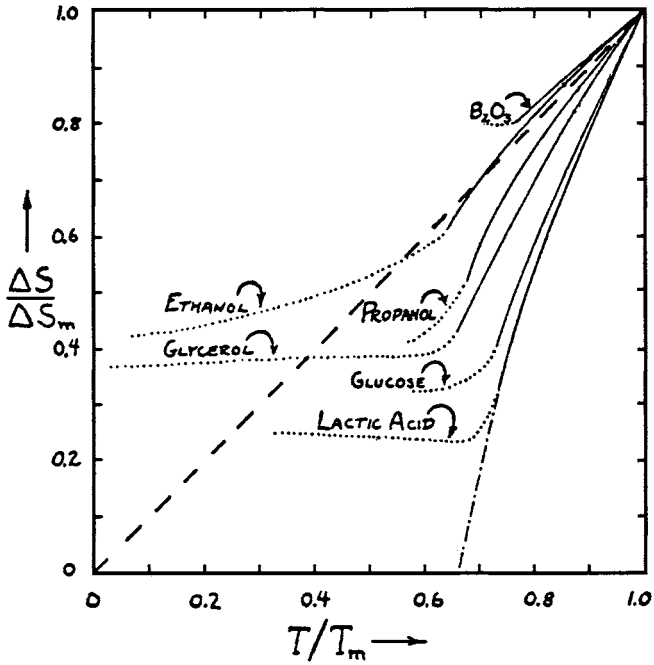

FIG. 5. Temperature dependence of the entropy difference between various supercooled liquids and their stable crystals, ΔS. ΔS_m is the entropy change upon melting, and T_m is the melting temperature. (Reprinted with permission from W. Kauzmann. The nature of the glassy state and the behavior of liquids at low temperatures. *Chem. Rev.* (1948); 43:219. Copyright © 1948, American Chemical Society.)

upon further cooling. This violation of the Third Law of Thermodynamics[3] is known as *Kauzmann's paradox,* although it was first noted by Simon (1931) (Wolynes, 1988).

The entropy crisis described in the preceding paragraph is the result of an extrapolation. With the exception of ^{3}He and ^{4}He (Wilks, 1967),[4] there is no known substance for which a Kauzmann temperature is actually reached. Nevertheless, the extrapolation needed to provoke a conflict with the Third Law is indeed modest for many substances (Angell, 1997), and what intervenes to thwart the imminent crisis is a kinetic phenomenon, the laboratory glass transition. This suggests a connection between the kinetics and

[3] Negative entropies are inconsistent with Boltzmann's formula, $S = k \ln \Omega$, where Ω denotes the number of quantum states corresponding to a given energy, volume, and mass.

[4] ^{4}He is a liquid at 0 K and 1 bar (liquid HeII); its equilibrium freezing pressure at 0 K is 26 bar. At this point, the entropies of the liquid and the crystal are equal, and this is therefore a Kauzmann point. The melting curves of both ^{3}He and ^{4}He exhibit pressure minima: these occur at ca. 0.32 K (^{3}He) and 0.8 K (^{4}He). These are also equal-entropy (Kauzmann) points.

the thermodynamics of glasses (Wolynes, 1988), a striking manifestation of which is the fact that fragile glass-formers behave like lactic acid in Fig. 5, their entropy of fusion being rapidly consumed upon supercooling (Ito *et al.*, 1999). Equally intriguing is the fact that for many fragile glass-formers, T_K, a thermodynamic quantity obtained from calorimetric measurements, is close to T_0, a dynamic quantity obtained from transport property measurements (Angell, 1997) [T_0 is the singular temperature where the VTF equation, Eq. (1), predicts complete structural arrest to occur]. Although the validity of extrapolations leading to entropy crises has been questioned (Stillinger, 1988), the situation depicted in Fig. 5 for fragile liquids such as lactic acid prompts inquiry into whether the laboratory glass transition is a kinetically controlled manifestation of an underlying thermodynamic transition, the ideal glass transition (Gibbs and DiMarzio, 1958). The proper role of thermodynamics, and its connection with kinetics, are major open questions in the physics of glasses.

The translational and rotational motion of a Brownian particle immersed in a fluid continuum is well described by the Stokes–Einstein and Debye equations, respectively,

$$D = k_B T/6\pi\eta a \tag{4}$$

$$D_r = k_B T/8\pi\eta a^3, \tag{5}$$

where D is the particle's translational diffusion coefficient, k_B is Boltzmann's constant, η is the fluid's viscosity, a is the radius of the Brownian particle, and D_r is its rotational diffusion coefficient.[5] Surprisingly, these equations hold down to the molecular level, and they have, accordingly, found widespread application in the interpretation and correlation of data on both tracer and self-diffusion in liquids. If account is taken of boundary conditions and molecular shape effects, the Stokes–Einstein–Debye relations are often accurate to within a factor of 2 (Cicerone and Ediger, 1996) provided $T \geq T_m$. In contrast, it is found experimentally that in supercooled liquids the Stokes–Einstein relationship breaks down around $1.2T_g$ (Fujara *et al.*, 1992; Cicerone and Ediger, 1995, 1996). Below this temperature, translational motion (both probe and self-diffusivity) is faster than predicted by the Stokes–Einstein equation by factors that become at least as high as 100 near T_g (Stillinger and Hodgdon, 1996). Note that this breakdown is in the direction opposite to that which would be predicted by invoking a growth in the effective size of molecules due to increasingly cooperative rearrangements upon supercooling. The inverse relationship between rotational diffusion and viscosity, however, continues to be accurately obeyed. This means that, upon cooling

[5] The numerical coefficients 6 and 8 in Eqs. (4) and (5) correspond to no slip at the fluid–particle interface. Other boundary conditions result in different numerical constants [e.g., 4 in Eq. (4) for fluid–particle slip].

below ca. $1.2T_g$, molecules translate increasingly faster than expected based on the known viscosity, and they also translate more for every rotation they execute. Although a plausible interpretation of the data has been offered invoking spatially heterogeneous dynamics (Cicerone and Ediger, 1995, 1996; Stillinger and Hodgdon, 1996), this remains a very active area of research because a definitive explanation of experimental observations does not exist (Wang and Ediger, 1999; Cicerone and Ediger, 1995, 1996; Hinze *et al.,* 1999; Liu and Oppenheim, 1996; Tarjus and Kivelson, 1995).

Sophisticated theoretical tools and experimental protocols exist for the characterization of crystalline structure (Kittel, 1966). The situation is quite different with disordered materials. The quantitative description of glassy structure is an important open problem. Ideally, this description should be based on *structural order parameters* that vary continuously between 0 (complete randomness) and 1 (perfect order). These order parameters should track specific types of order, such as translational order (the tendency of molecules to occupy preferred positions in space) and orientational order (the tendency of anisotropic molecules to adopt a preferred orientation). The development of an analytical framework for quantifying disorder is still in its infancy (Ziman, 1979; Zallen, 1983; Torquato *et al.,* 2000; Truskett *et al.,* 2000). Progress in this area could lead to advances in the early detection of tumors (Hama *et al.,* 1999), the design of transdermal drug delivery systems (Brinon *et al.,* 1999), the prediction and characterization of flow through porous media and packed beds (Bryant and Blunt, 1992; Torquato, 1994; Sahimi, 1995), the efficient handling and processing of powders and granular materials (Shahinpoor, 1980), and the characterization and processing of foods (Blanshard and Lillford, 1993).

Other important unanswered questions were mentioned in Section I.A (origin of energy barriers that give rise to Arrhenius and super-Arrhenius behavior close to T_g, origin of stretched exponential dynamics). Clearly, there are large gaps in our knowledge of disordered solids and the liquids from which they are commonly formed. In this article we review recent theoretical progress toward an improved understanding of glasses and supercooled liquids resulting from the application of the energy landscape formalism and statistical geometry.

C. Structure of This Article

In Section II we define energy landscapes, and we present the formalism that relates potential energy minima to the thermal properties of supercooled liquids and glasses. Section III discusses the characterization of voids in dense particle packings, and how this approach, combined with energy minimization techniques, can yield powerful new insights into the mechanical

properties of glasses. Also included in this section is a discussion of recent work on the characterization of disorder and its application to model hard-sphere glasses. The intriguing connection between the dynamics and the thermodynamics of the glassy state is discussed in Section IV. It is shown there that understanding the manner in which a supercooled liquid samples its potential energy surface provides powerful insight into stretched exponential behavior, low-temperature breakdown of the Stokes–Einstein behavior, and the connection between entropy and viscous slowdown. Section V introduces the statistical description of an energy landscape and derives its connection to a macroscopic system's thermodynamic properties. It also suggests experimental and computational routes to the investigation of landscape statistics. Section VI summarizes the significant progress that has occurred in recent years through the application of energy landscape and statistical geometry concepts to the understanding of disordered solids and the liquids from which they are formed, and lists major open questions.

II. The Energy Landscape

The interactions operating among the atoms, ions, or molecules of any material system play a dominant role in determining static and dynamic properties of that system. Dilute gases are easy to analyze, at least conceptually, in that interactions occur primarily in isolated small clusters (pairs, triplets, etc.). But the situation is qualitatively different and far more challenging for fluid and solid condensed phases: virtually every particle remains in constant contact with many neighbors, and the system presents a volume-spanning macroscopic cluster. In particular, this is true for the supercooled liquids and glasses that form the subject of this article.

Under these condensed-phase conditions it is natural to consider the full N-body potential energy function $\Phi(\mathbf{r}_1 \ldots \mathbf{r}_N)$ for the material system of interest and to seek to describe the way its details generate the wide variety of collective thermodynamic and kinetic phenomena that have been experimentally observed in condensed matter. For the remainder of this section we suppose that all N particles are the same chemical species and that vectors $\mathbf{r}_i$ comprise all relevant position, orientation, conformation, and vibration coordinates. For the moment, volume V will be constant.

Except for configurations with coincidence of nuclei, Φ is bounded and arbitrarily differentiable in all its coordinates. Therefore it is useful to examine the geometry of the smooth hypersurface generated in the multidimensional space of variables,

$$\mathbf{r}_1, \mathbf{r}_2, \ldots, \mathbf{r}_N, \Phi. \tag{6}$$

This hypersurface constitutes the system's energy landscape. If ν is the number of internal degrees of freedom per particle (orientation, conformation, etc.), then the dimension of the space (6) will be

$$(3 + \nu)N + 1. \tag{7}$$

Theoretical study of the N-body system now focuses on the Φ hypersurface topography, or, more colloquially, its "rugged landscape." Specific landscape characteristics of interest are the number of minima and their distribution and the nature of saddle points (transition states) throughout the landscape. A schematic illustration of an energy landscape is shown in Fig. 6 (Stillinger, 1995).

The early work of Goldstein (1965, 1969) is a prescient precursor of the topographic viewpoint of condensed phases (Stillinger, 1995) illustrated schematically in Fig. 6. Landscape-based ideas have since found fruitful application to a wide variety of problems, such as protein folding (Frauenfelder *et al.*, 1991; Wolynes, 1992; Abkevich *et al.*, 1994; Chan and Dill, 1994; Frauenfelder and Wolynes, 1994; Saven *et al.*, 1994; Wolynes *et al.*, 1995; Wang *et al.*, 1996; Plotkin *et al.*, 1996, 1997; Becker and Karplus, 1997; Dill and Chan, 1997; Wolynes, 1997), melting and freezing phenomena (LaViolette and Stillinger, 1985a; Patashinski and Ratner, 1997), the mechanical properties of glasses (Lacks, 1998; Malandro and Lacks, 1997, 1999; Utz *et al.*, 2001), shear-enhanced diffusion in liquids and colloidal suspensions (Malandro and

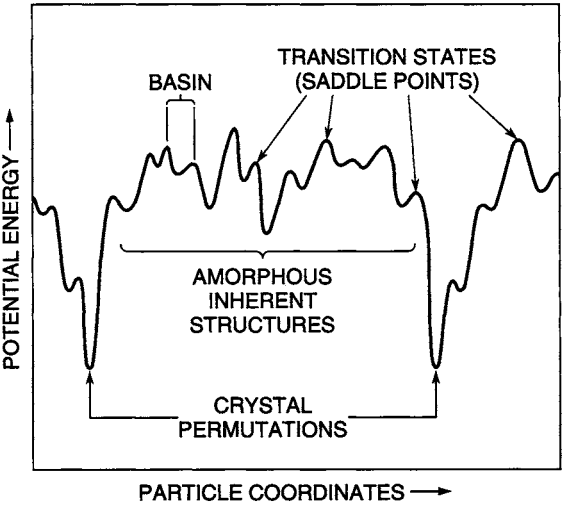

FIG. 6. Schematic illustration of an energy landscape for a many-particle system. The horizontal direction represents all configurational coordinates. (Reprinted with permission from F. H. Stillinger. A topographic view of supercooled liquids and glass formation. *Science* 1995; 267:1935. Copyright © 1995, American Association for the Advancement of Science.)

Lacks, 1998), the dynamics of supercooled liquids (Schulz, 1998; Sastry *et al.*, 1998a; Keyes, 1999), and economic optimization with complex cost functions. A useful collection of papers on this topic can be found in the volume edited by Frauenfelder *et al.* (1997). The landscape formalism presented in the rest of this section focuses on supercooled liquids and glasses.

Symmetries intrinsic to the N-body system lead to a partitioning of the configuration space into equivalent symmetry sectors. If γ is the symmetry number for each particle, the number of sectors is

$$\Gamma = N!\gamma^N, \tag{8}$$

where the first factor $N!$ accounts for the exchange permutations that are possible with the N identical particles. The potential energy landscape thus consists of many replicas of a primitive topographic parcel. In particular, each distinguishable Φ minimum and saddle point appears Γ times in the configuration space. The Φ local minima offer a conceptually simple way to describe the fine details of the energy landscape. The system configuration $\mathbf{r}_1 \ldots \mathbf{r}_N$ at any one of these minima by definition is one with overall mechanical stability: forces and torques on every particle vanish simultaneously. For this reason these discrete special configurations are often called "inherent structures" (Stillinger and Weber, 1982). It has been demonstrated (Stillinger, 1999) that in the large-system limit, the number of inherent structures in each symmetry sector rises exponentially with N, assuming that the number density N/V (>0) is held fixed.

Identification of inherent structures leads to a natural division of the multidimensional configuration space into nonoverlapping regions, one for each inherent structure, that cover the entire space. The most direct way to accomplish this is to use steepest descent mapping, defined by solutions to the equation set

$$d\mathbf{r}_i/ds = -\partial\Phi/\partial\mathbf{r}_i \qquad (1 \le i \le N; \qquad 0 \le s), \tag{9}$$

where s is a "progress variable." The locus of all points that connect to a given inherent structure by solutions to Eq. (9) define the "basin of attraction" for that inherent structure (see Fig. 6). These basins contain all configurations that can be viewed as vibrationally distorted versions of the respective inherent structures. Small intrabasin displacements from the inherent structure minimum will be accurately described as harmonic motions, while those of higher amplitude that carry the system configuration close to a shared boundary between two basins will tend to be strongly anharmonic.

The deepest basin in each symmetry sector corresponds to the most nearly perfect crystalline arrangement of the N particles in the available volume V for that crystal structure that is stable at 0 K. If V is conformal with that crystal structure, and N is one of the corresponding "magic number" integers, then the inherent structure at the bottom of these Γ deepest basins will be

that of a defect-free crystal. Small displacement then are conventionally described as composed of independent phonons (Ashcroft and Mermin, 1976). The simplest structural excitations from this defect-free state to neighboring higher-lying basins involve localized rearrangents that produce point defects in the crystal and are expected to occur in $O(N)$ different real-space locations or, equivalently, along the same number of distinct directions in the multidimensional configuration space. At the other extreme each symmetry sector will contain one (or more) highest-lying basins. These surround inherent structures that are energetically the least favorable ways to arrange the N particles in space to achieve mechanical stability. In most cases of interest this requirement is expected to produce an amorphous particle deposit.

The potential energy range between the lowest- and the highest-lying basin bottoms is an extensive property of the N-body system. In view of the fact that exponentially many (in N) distinct inherent structures are crowded in between these limits, it is sensible to consider the statistical distribution of basins in a symmetry sector by depth. Let

$$\phi = \Phi/N \tag{10}$$

be an intensive order parameter for classifying basins by depth (Speedy, 1999). We can write the following expression, asymptotically valid in the large system limit, for that distribution (Stillinger, 1999)

$$\frac{d\Omega}{d\phi} = C \exp[N\sigma(\phi)], \tag{11}$$

where $d\Omega$ denotes the number of inherent structures with a depth (on a per particle basis) between ϕ and $\phi \pm d\phi/2$. Here C and $\sigma(\phi)$ are independent of N, with the former a scale factor with dimension inverse energy. If ϕ_c and ϕ_w, respectively, stand for the ϕ values of the lowest-lying (crystalline) and the highest-lying (worst) inherent structures, then $\sigma(\phi)$, the basin enumeration function, will be nonnegative and continuous between these limits, presumably with

$$\begin{aligned} \sigma(\phi_c) &= 0 \\ \sigma(\phi_w) &= 0 \end{aligned} \tag{12}$$

and passing through at least one maximum between these limits.

A vibrational partition function can be assigned to each basin α (Debenedetti *et al.*, 1999),

$$Q_{v,\alpha} = \Lambda^{-N}(\beta) \int_{B(\alpha)} d\mathbf{r}_1 \ldots d\mathbf{r}_N \exp\{\beta[\Phi_\alpha - \Phi(\mathbf{r}_1 \ldots \mathbf{r}_N)]\}, \tag{13}$$

where Λ comes from integration over conjugate momenta, $\beta = 1/k_B T$, $B(\alpha)$ is the region occupied by basin α in the multidimensional configuration space,

and Φ_α is the potential energy of the embedded inherent structure. While these $Q_{\nu,\alpha}$ will surely vary from basin to basin, it is their average dependence on order parameter ϕ that is most significant. For that reason, select a narrow range $\phi \pm \varepsilon$ (ε eventually to go to zero after the large-system limit), and compute the vibrational free energy per particle $a^\nu(\phi, \beta)$ as the following arithmetic mean over this narrow basin fraction:

$$\exp[-N\beta a^\nu(\beta, \phi)] = \langle Q_{\nu,\alpha}(\beta)\rangle_{\phi\pm\varepsilon}. \tag{14}$$

With the benefit of the σ and a^ν definitions, it becomes possible to express the canonical partition function for the N-particle system as a simple ϕ integral (Stillinger and Weber, 1982),

$$\begin{aligned} Q(N, V, \beta) &= \Lambda^{-N} \int d\mathbf{r}_1 \ldots d\mathbf{r}_N \exp[-\beta\Phi(\mathbf{r}_1 \ldots \mathbf{r}_N)] \\ &= C \int_{\phi_c}^{\phi_u} d\phi \exp\{N[\sigma(\phi) - \beta\phi - \beta a^\nu(\beta, \phi)]\} \\ &\equiv \exp(-\beta A), \end{aligned} \tag{15}$$

giving the Helmholtz free energy A as usual.[6] The large-N limit causes the integrand, and thus the integral itself, to be dominated by the neighborhood of the maximum of the bracketed combination appearing in the exponent. Let $\bar{\phi}(\beta)$ denote the value of the order parameter which produces the integrand maximum at the temperature under consideration. The Helmholtz free energy per particle then possesses the simple form

$$-\beta A(\beta)/N = \sigma[\bar{\phi}(\beta)] - \beta\bar{\phi}(\beta) - \beta a^\nu[\beta, \bar{\phi}(\beta)]. \tag{16}$$

Temperature variations cause $\bar{\phi}$ to shift, thereby accessing different positions of the basin-depth distribution function (11). In any event $\bar{\phi}(\beta)$ identifies the set of basins preferentially inhabited at the chosen temperature. As will be shown in Section V, $\sigma(\bar{\phi})$ for low molecular weight substances in the liquid state tends to fall in the range 1 to 10 (see also Stillinger, 1998; Speedy, 1999).

If N is equal to Avogadro's number, the single-sector distribution (11) will contain an overwhelmingly dominating factor approximately equal to

$$10^{10^{23}}. \tag{17}$$

With any reasonable estimate for the kinetic rate of interbasin transitions, it would take far longer than the age of the Universe for the 1-mol system

[6] Both σ and a^ν depend on density. The notation in (15) and (16) corresponds to isochoric exploration of the landscape.

to visit all of the basins that are relevant for the given temperature (even if no returns to previously visited basins occurred). Given this situation, it is important to understand that thermal equilibrium on the laboratory time scale involves sampling only a tiny, but *representative,* subset of the basins designated $\sigma(\bar{\phi})$.

Equation (16) for the Helmholtz free energy shows that equilibrium thermodynamic data intrinsically entangles basin numeration (σ) and vibration (a^{ν}) aspects of the N-body system (Stillinger *et al.,* 1998; Stillinger and Debenedetti, 1999). Partial disentanglement becomes possible upon leaving the equilibrium domain. Specifically, very rapid temperature quenches from an equilibrium state at T can trap the system in a basin or small group of neighboring basins contained in $\sigma[\bar{\phi}(\beta)]$. Indeed, the ideal limit of infinitely rapid temperature quench to 0 K would be equivalent to the steepest descent mapping that defines the inherent structures and their basins. In this way the energies and structures of individual inherent structures could in principle be determined.

Crystal nucleation from a pure melt in the neighborhood of its thermodynamic freezing point is kinetically sluggish for most substances, thus permitting at least some amount of liquid supercooling. This circumstance violates the "representative sampling" mentioned above, by excluding those basins whose inherent structures contain some significant amount of crystalline order. Those basins not so excluded correspond to amorphous inherent structures, whose depth distribution could be described by $\sigma_{\mathrm{a}}(\phi)$, where

$$\sigma_{\mathrm{a}}(\phi) \leq \sigma(\phi). \tag{18}$$

A free energy expression for the metastable supercooled liquid, exactly analogous to that shown in Eq. (16), now becomes applicable:

$$-\beta A_{\mathrm{a}}(\beta)/N = \sigma_{\mathrm{a}}[\bar{\phi}_{\mathrm{a}}(\beta)] - \beta\bar{\phi}_{\mathrm{a}}(\beta) - \beta a_{\mathrm{a}}^{\nu}[\beta, \bar{\phi}_{\mathrm{a}}(\beta)]. \tag{19}$$

As indicated, the vibrational free energy requires an average over the restricted basin set, and $\bar{\phi}_{\mathrm{a}}(\beta)$ is the statistically preferred depth in that set obtained by maximizing this modified expression. Of course, even this extension (19) breaks down at and below a glass transition temperature.

Although the various considerations covered in this section could be used to determine some basic characteristics of the multidimensional energy landscape, much would remain undetermined. In particular, details about interbasin transition states and about the overall arrangement of the basins of various depths have not yet been illuminated. The time-dependent phenomena considered in Section IV can supply at least some of the desired information.

The development thus far has implicitly assumed constant-volume (isochoric) conditions. Constant-pressure (isobaric) conditions are also

experimentally important and can simply be handled by appending volume V, now variable, to the list of configurational coordinates:

$$\mathbf{r}_1, \mathbf{r}_2, \ldots, \mathbf{r}_N, V. \tag{20}$$

At the same time, the pressure–volume product should be appended to the potential energy function

$$\Psi(\mathbf{r}_1 \ldots \mathbf{r}_N, V) = \Phi(\mathbf{r}_1 \ldots \mathbf{r}_N) + pV \tag{21}$$

to yield a "potential enthalpy." The dimension of the augmented configuration space thus increases by unity, and the "rugged landscape" is that of Ψ. All of the preceding considerations adapt to this alternative circumstance, with basins distributed in depth by the intensive order parameter,

$$\psi = \Psi/N, \tag{22}$$

the analogue of Eq. (10).

III. Statistical Geometry and Structure

Unlike crystalline solids, supercooled liquids and glasses are characterized by a topological complexity at the molecular level that eliminates long-range periodic order. This should not be surprising given that experimental protocols for glass formation, by design, frustrate the natural tendency of substances to crystallize at low temperatures. Moreover, since supercooled liquids "fall out of equilibrium" upon vitrification, the details of the resulting glassy structures depend sensitively on the mode of preparation, i.e., on the thermal processing history (Angell, 1995; Debenedetti, 1996).

Although long-range order is noticeably absent in liquids and glasses, species-dependent intermolecular interactions (e.g., "hard-core" repulsion or strong molecular association) inevitably promote the buildup of substantial short-range order in condensed phases, as evidenced by diffraction experiments (Zallen, 1983) and molecular simulation (Angell *et al.*, 1981). Although the molecular-based study of liquids and their mixtures is an important component of modern chemical engineering research (e.g., Theodorou, 1994; Prausnitz, 1996; Gubbins and Quirke, 1996, Debenedetti, 1996; Davis, 1996; Deem, 1998), comparatively less effort has been devoted to the problem of characterizing and quantifying structure in disordered phases.[7]

In this section, we examine recent developments in the description and interpretation of the underlying geometric structure of the liquid and glassy

[7] The use of fractal and percolation concepts to characterize pore-space topology (Sahimi, 1993) is a notable exception.

state. In particular, we focus on the application of powerful new theoretical and algorithmic tools to interrogate the nature of molecular ordering and the geometry of the intervening void space in model systems.

A. Void Geometry and Connections to the Energy Landscape

The complex geometry of the pore structure, or alternatively the *void space,* in a material (including its volume, surface area, and connectivity) can play a central role in determining many of its physical properties. Examples include transport processes in porous media (Torquato, 1991; Reiss, 1992); permeability, flow, and diffusion of fluids in packed beds (Thompson and Fogler 1997); mass transfer in polymeric glasses (Greenfield and Theodorou, 1993); adsorption in zeolite crystals (Dodd and Theodorou, 1991); stability and function of proteins and nucleic acids (Liang *et al.,* 1998); bubble nucleation (Shen and Debenedetti, 1999); the thermodynamics of fluids (Speedy, 1980; Sastry *et al.,* 1998b); and the nature of phase transitions in condensed-phase systems (Reiss and Hammerich, 1986; Bowles and Corti, 2000).

Given the diversity of relevant applications, it is not surprising that the characterization of voids in disordered systems has an appreciable history, which can be traced back to primitive "hole" theories of the liquid state (Frenkel, 1955; Ono and Kondo, 1960). While the early theories offer an admittedly rudimentary "lattice" description of voids, recent computational advances permit an exact (and highly efficient) characterization of the continuum void geometry present in particle packings in two (Rintoul and Torquato, 1995) and three dimensions (Sastry *et al.,* 1997a).

An important recent development in the rigorous characterization of disordered materials is the geometric algorithm of Sastry *et al.* (1997a). It allows the identification of disconnected cavities in monodisperse and polydisperse sphere packings, and the exact determination of the volume and surface area of these packings (Fig. 7).[8] This algorithm has proven to be a powerful tool for probing the void geometry of metastable liquids and glasses (Sastry *et al.,* 1997b, 1998b; Shen and Debenedetti, 1999; Vishnyakov *et al.,* 2000; Utz *et al.,* 2001). It should be mentioned in passing that some of the void quantities mentioned above can, at least in principle, be determined using standard Monte Carlo sampling methods (Shah *et al.,* 1989). However,

[8] In any sphere packing, it is possible to partition the given volume into occupied and available space. The former is the union of all the exclusion spheres, and the latter is its complement, namely, the volume available for the placement of the center of an additional sphere. The exclusion region of a sphere of diameter σ is a concentric sphere of radius σ. Exclusion spheres can overlap. At a high enough density, the available space is in general composed of disconnected cavities.

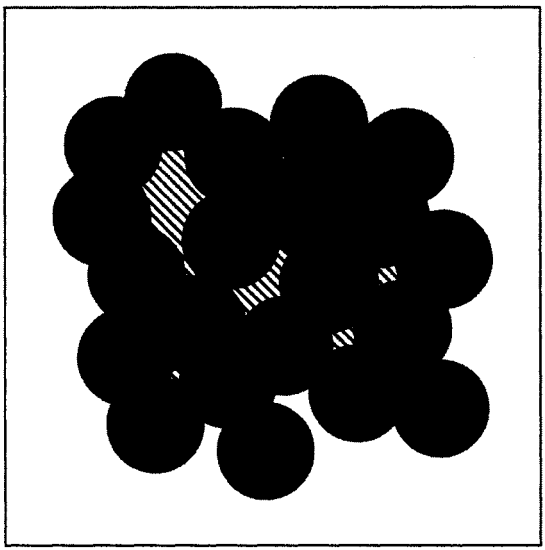

FIG. 7. A random configuration of atoms (black) surrounded by exclusion spheres (gray). The disconnected pockets of space that lie outside of the generally overlapping exclusion spheres are termed "cavities" (cross-hatched). A natural choice for the effective exclusion radius for the Lennard–Jones fluid is $r_{ex} = \sigma$, the Lennard–Jones diameter.

stochastic schemes become unsatisfactory at high density, when the volume fraction of the void space is small (Rintoul and Torquato, 1995).

The geometric algorithm of Sastry *et al.* (1997a) is based on a Voronoi–Delaunay tessellation[9] (Tanemura *et al.*, 1983). It consists of three basic steps.

(a) *Identification of cavities.* This is accomplished by obtaining the percolation clusters of Voronoi edges in the void.
(b) *Identification of polyhedra enclosing the cavities.* The union of Delaunay tetrahedra dual to the Voronoi vertices in a cavity provides an upper bound on the cavity volume.
(c) *Determination of cavity volume and surface area.* This is done by a systematic decomposition of each Delaunay tetrahedron into 24 subunits.

For details on each of these steps, interested readers should consult the original paper (Sastry *et al.*, 1997a).

[9] The Voronoi tessellation divides space into polyhedral regions that are closer to the center of a given particle than to any other. Joining pairs of particle centers whose Voronoi polyhedra share a face yields a dual tessellation of space into Delaunay simplices.

The application of this algorithm to explore the morphology of Lennard–Jones inherent structures has yielded new insights into the fundamental nature of the glass transition and suggested a possible and previously unsuspected connection with bubble nucleation in liquids under tension. Sastry *et al.* (1997b) investigated the inherent structures of a Lennard–Jones system with smoothly truncated interactions. The results from this study, together with previous work on single-component, nonassociating liquids (Weber and Stillinger, 1984; LaViolette and Stillinger, 1985b; Stillinger and Weber, 1985; LaViolette, 1989; Stillinger and Stillinger, 1997), reveal that the packing geometry and energy of the inherent structures are virtually independent of the equilibration temperature. In contrast, it is known that the energy landscape exhibits a rich and highly nontrivial density dependence (LaViolette, 1989; Sastry *et al.*, 1997b; Malandro and Lacks, 1997). It is precisely the exploration of this density dependence that has yielded important new information on the glass transition, metastability, and nucleation (Sastry *et al.*, 1997b; Debenedetti *et al.*, 1999).

In the case of the shifted-force Lennard–Jones system, Sastry *et al.* (1997b), confirming earlier similar observations by LaViolette (1989) showed that inherent structure morphologies can divided into three distinct intervals in density:

$$\begin{aligned} &\text{A:} \quad 0.99 < \rho\sigma^3 \\ &\text{B:} \quad 0.89 < \rho\sigma^3 < 0.99 \\ &\text{C:} \quad \rho\sigma^3 < 0.89. \end{aligned} \tag{23}$$

Here, σ and ε are the familiar Lennard–Jones parameters, ρ is the number density ($\rho = N/V$), N is the number of molecules, and V is the total volume. As a point of reference, the reduced triple-point density and the critical-point density for the liquid in this model occur at $\rho_{\mathrm{TP}}\sigma^3 = 0.815$ and, $\rho_c\sigma^3 = 0.323$, respectively (the corresponding critical pressure and temperature are $P_c\sigma^3/\varepsilon = 0.0805$ and $kT_c/\varepsilon = 0.935$) (Errington, 2000).

Figure 8 illustrates the nonmonotonic density dependence of the average pressure in the inherent structures. In the first of these intervals (A), the inherent structures exist at a positive pressure (although the pressure is smaller in magnitude than for the equilibrated fluid configurations at the same density). Interval B contains inherent structures in tension (i.e., at negative pressure). Note that the magnitude of the tension in these structures increases with decreasing density, approaching a state of maximum isotropic tensile strength at a reduced density of

$$\rho\sigma^3 = 0.89. \tag{24}$$

Interval C also shows inherent structures with negative pressures; however,

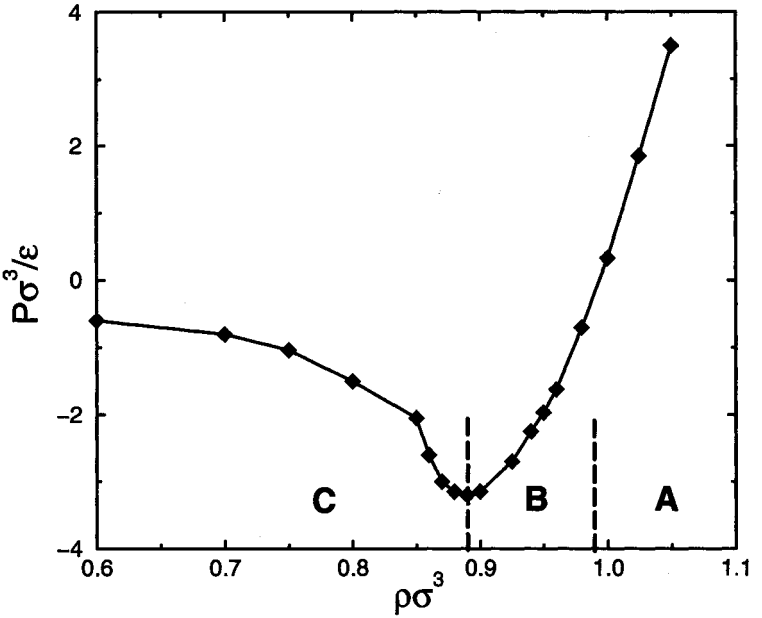

FIG. 8. Density variation of the inherent structure pressure for a fluid with a smoothly truncated Lennard–Jones potential (Sastry *et al.*, 1997b). Regions A, B, and C identify distinguishing density intervals for the inherent structures discussed in the text.

in this density range, the sustained tension is clearly reduced with decreasing density.

A detailed geometric analysis (Sastry *et al.*, 1997b) of the void space in the inherent structures reveals that the density of maximum tension ρ_s has special significance. It represents the density below which the attractive interactions in the system are unable to sustain a mechanically stable packing that is amorphous, isotropic, and statistically homogeneous. This density, known as the Sastry density, is an important material characteristic: since a glass is a liquid arrested at (or close to) a mechanically stable configuration, or inherent structure, we reach the important conclusion that it is not possible to form a homogeneous glass below a material's Sastry density.

Expanding the system to lower densities literally shreds the inherent structures into several densely packed regions threaded by large system-spanning voids. Given that equilibrium liquid configurations in interval C "fracture" as they are continuously deformed into their respective local potential energy minima, it is not surprising that the tension sustained in the resulting heterogeneous inherent structures declines with decreasing density. Although extremely low-density inherent structures ($\rho\sigma^3 < 0.60$) have not

been systematically investigated, the rational expectation is that the tension will monotonically diminish as the density approaches zero. The geometry of the resulting mechanically stable structures should be extremely tenuous, perhaps resembling aerogels (Fricke, 1986; Kieffer and Angell, 1988; Stillinger, 2001). Finally, we point out that the structures at $\rho\sigma^3 \approx 0.99$ experience zero pressure and may indeed exhibit features similar to amorphous deposits prepared from low-pressure vapor deposition of single-component substances.

The shape of the pressure versus density curve in Fig. 8 is reminiscent of the metastable pressure isotherms which cross through the vapor–liquid coexistence region, as predicted by the van der Waals equation of state and other mean-field theories (Hirschfelder *et al.,* 1954). In fact, Sastry *et al.* (1997b) argued that the curve shown in Fig. 8 represents the true zero-temperature limit of such metastable isotherms in the smoothly truncated Lennard–Jones fluid, and hence the extremum of the $p(\rho)$ curve at the Sastry density is the low-temperature limit of the spinodal curve along which the superheated liquid becomes mechanically unstable with respect to the vapor. This identification is supported by mean-field calculations on a number of model systems (Debenedetti *et al.,* 1999), as discussed in more detail in Section V. The important point here is the intriguing connection and possible convergence of the limit of stability upon superheating and the ultimate vitrification limit upon supercooling.

The results of the simple Lennard–Jones fluid invite the following basic question about materials: What aspects of molecular architecture (e.g., shape, symmetry, flexibility, etc.) are crucial in determining the details of the energy landscape and, ultimately, the structural and mechanical features of the liquid and the glass? To shed some light on this important issue, the density dependencies of various properties of the energy landscape have been recently explored for molecular models of ethane, pentane, and cyclopentane (Utz *et al.,* 2001). Interestingly, the molecular liquids were found to be very similar to the Lennard–Jones fluid in one respect: the "equation of state" of the energy landscape, i.e., the relationship between inherent structure pressure and bulk density, appears to be virtually independent of temperature. The extent to which molecular factors such as chain length and branching will alter this picture is a fascinating open question. Details of the void geometry reveal another interesting feature, namely, that the surfaces of the inherent structure cavities that form below ρ_s (the density of maximum tensile strength) are enriched in end groups (Utz *et al.,* 2001). This finding may have important implications for understanding the mechanisms for cavitation in chain-like fluids.

An analogous but much richer behavior is expected to be exhibited by good glass-forming materials. As discussed in more detail in Section IV, the mean inherent structure energy in these systems can show a significant

dependence on equilibration temperature (Sastry *et al.,* 1998a). Furthermore, the average inherent structure pressure and the underlying void geometry are expected to be notably temperature dependent, replacing the simple result shown for the Lennard–Jones fluid in Fig. 8 with a family of curves. The prediction, although (to the best of our knowledge) not yet tested experimentally, is that lower equilibration temperatures will result in inherent structures which are more capable of resisting dilatational fracture.

Finally, we note that the specific, directional hydrogen bonds present in liquid water and aqueous solutions confer complexity to their underlying energy landscapes. The wide diversity of inherent structures in water is evidenced experimentally by the existence of multiple crystalline polymorphs (Eisenberg and Kauzmann, 1969), clathrate networks (Davidson, 1973), and high- and low-density amorphous solids (Mishima and Stanley, 1998). Recent simulations of a model for liquid water (Roberts *et al.,* 1999) indicate that its energy landscape is indeed rugged and diverse. Not only are the properties of the inherent structures temperature dependent, but also Roberts *et al.* (1999) demonstrate that in some density ranges the amorphous inherent structures can attain lower potential energies than the ground states of the pure crystalline forms. Although the structural features underlying the energy landscape have not yet been elucidated, this observed behavior suggests the possibility of a microscopic interpretation of many of water's anomalous features, including the observed polyamorphic transition between its glassy phases (Mishima and Stanley, 1998) and the fragile-to-strong transition (Ito *et al.,* 1999) as water is supercooled to its vitreous form.

The systematic investigation of structure, void distribution, and morphology in mechanically stable packings (inherent structures) is still in its infancy. Yet what has been learned so far about the mechanical properties of molecular glasses (Utz *et al.,* 2001), absolute limits to vitrification (Debenedetti *et al.,* 1999), the phase behavior of metastable water (Roberts *et al.,* 1999), and bubble nucleation (Sastry *et al.,* 1997b; Utz *et al.,* 2001) suggests that exploring the connection between statistical geometry and energy landscapes is a powerful route to understanding and eventually predicting the thermal and volumetric properties of supercooled liquids and glasses.

B. Quantifying Molecular Disorder in Equilibrium and Glassy Systems

Although significant theoretical and computational progress has yielded valuable insights into the morphology of void space in supercooled liquids and glasses, much remains to be clarified about the nature of molecular-level disorder present in amorphous systems. Glassy systems are of special

interest because they exhibit rich and complex microstructures with pronounced molecular correlations, yet they lack the long-range order characteristic of crystalline solids. In this subsection we focus on recent advances in the description of simple models of disordered condensed phases; however, it should be emphasized that the general problem of describing quantitatively the types of disorder that nature exhibits over a wide variety of length scales (e.g., porous rock, plant structure, tissues) is of enormous scientific and technical importance (Cusack, 1987; Laughlin *et al.*, 2000; Truskett *et al.*, 2000).

At one extreme, a truly random system, by definition, can exhibit no molecular correlations, be they positional, orientational, or conformational—its structure is that of an ideal gas. On the other hand, a perfect periodic crystalline array is a manifestation of perfect order. Our experience with molecular systems in Nature indicates that these extremes exist only as limiting concepts. Between the ideal gas and the perfect crystal lie imperfect gases, liquids (both stable and metastable), liquid crystals, defective crystals, incommensurate structures, quasicrystals, and a variety of structures that organize by nonequilibrium processes, such as glasses and materials formed by irreversible adsorption onto a substrate. Depending on the point of view, all such systems exhibit a certain degree of order (or disorder), and the differences between them can be remarkably subtle. For instance, the problem of distinguishing between the structure of dense glasses and that of polycrystalline materials remains a significant challenge for materials scientists and engineers (Zallen, 1983; Cusack, 1987).

To describe quantitatively the disorder present in a material, it is often convenient to introduce a *structural order parameter*. This term refers to a metric that can detect the development of order in a many-body system, perhaps by employing the tools of pattern recognition (Brostow *et al.*, 1998). In many cases, such a measure is constructed to serve as a "reaction coordinate" for a thermodynamic phase transition (van Duijneveldt and Frenkel, 1992). However, since the form of the order parameter clearly depends on the phenomenon of interest, the development of such measures can be a difficult and subtle matter.

Given that the supercooling of a liquid can lead to structurally distinct possibilities (the stable crystal or a glass), structural order parameters are especially valuable in understanding low-temperature metastability. In particular, it has been demonstrated (van Duijneveldt and Frenkel, 1992) that the *bond-orientational* order parameters introduced by Steinhardt *et al.* (1983) are well suited for detecting crystalline order in computer simulations of simple supercooled liquids. The bond-orientational order parameters are so named because they focus on the spatial orientation of imaginary "bonds" that connect molecules to their nearest neighbors defined as above with

the Voronoi–Delaunay tesselation. If these bond orientations persist over a macroscopic distance in the sample (e.g., as they do in a perfect crystal), then the system is said to be *bond-orientationally ordered.*

Of particular interest is the specific bond-orientational order parameter given by

$$Q_6 = \sqrt{\frac{4\pi}{13} \sum_{m=-6}^{6} |\bar{Y}_{6m}|^2}, \tag{25}$$

where $\bar{Y}_{6m}$ represents the spherical harmonic associated with the orientation (θ, ϕ) of a bond in the laboratory reference frame, and the overbar indicates an average over all bonds in the sample. The parameter Q_6 has the desirable property that it vanishes for a completely random system in the infinite-volume limit (Rintoul and Torquato, 1996), whereas it is significantly larger when crystallites are present, attaining its maximum value for space-filling structures ($Q_6^{\mathrm{FCC}} = 0.5745$ in the perfect face-centered cubic (FCC) lattice). Q_6 is also large for a number of alternative crystalline structures, including the body-centered cubic, the simple cubic, and the hexagonal lattices (Steinhardt *et al.,* 1983). This property renders Q_6 an extremely valuable tool for investigating metastability and crystal growth in computer simulations of simple atomic fluids and colloidal suspensions (Rein ten Wolde *et al.,* 1996; Rintoul and Torquato, 1996; Lacks and Wienhoff, 1999; Huitema *et al.,* 1999; Richard *et al.,* 1999). In what follows, we normalize the bond-orientational order parameter Q_6 by its value in the perfect FCC lattice, $\Theta = Q_6/Q_6^{\mathrm{FCC}}$.

In contrast to the bond-orientational order parameters mentioned above, scalar measures for translational order [that is, of the tendency of particles (atoms, molecules) to adopt preferential pair distances in space] have not been well studied. However, a number of simple metrics have been introduced recently (Truskett *et al.,* 2000; Torquato *et al.,* 2000, Errington and Debenedetti, 2001) to capture the degree of spatial ordering in a many-body system. In particular, the structural order parameter τ,

$$\tau = \left| \frac{\sum_{i=1}^{N_c} \left(n_i - n_i^{\mathrm{ideal}}\right)}{\sum_{i=1}^{N_c} \left(n_i^{\mathrm{crystal}} - n_i^{\mathrm{ideal}}\right)} \right|, \tag{26}$$

was constructed to measure the degree of translational order in a system relative to some relevant crystal lattice[10] (Truskett *et al.,* 2000; Torquato *et al.,* 2000). To understand the structural order parameter τ, we consider three systems with the same number density ρ: the system of interest, a completely

[10] The structural order parameter τ should not be confused with the relaxation time τ defined in Eq. (2).

random system (i.e., an ideal gas), and the reference crystal lattice. Here, n_i^{crystal} indicates the number of neighbors that are located in a molecule's ith neighbor shell (a distance r_i from the molecule) in the reference crystal lattice. Similarly, n_i^{ideal} refers to the average number of neighbors that are located at a distance r from a molecule [where $r_i - (a\delta/2) < r < r_i + (a\delta/2)$] in the ideal gas. Finally, n_i measures the number of neighbors that lie in that same spherical shell surrounding a molecule in the system of interest. As can be seen from (26), τ quantifies the degree of spatial ordering in the system of interest by "metering" its position between the two natural limits, the ideal gas ($\tau = 0$) and the perfect crystalline lattice ($\tau = 1$). In the above outline, $a = r_1$ (the first nearest-neighbor distance for the reference crystal), δ is a shell width parameter, and N_C is the total number of neighbor shells considered in the reference crystal.

The structural order parameter τ was originally introduced to investigate ordering in the hard-sphere system, for which the appropriate reference crystal structure is the FCC lattice (Torquato *et al.*, 2000). In that investigation, the first seven neighbor shells were considered ($N_c = 7$), allowing for a shell-width parameter of size $\delta = 0.196$. From a practical perspective, it was noted that consideration of more neighbor shells did not result in qualitatively different behavior for τ (Truskett *et al.*, 2000). We mention in passing that the approach outlined above is useful only if the relevant ordered state (i.e., the reference crystal structure) is known a priori. The development of robust structural order parameters that do not require such information, so-called *crystal-independent* measures, is an active area of research (Truskett *et al.*, 2000; Errington and Debenedetti, 2001).

We can gain some insight into the molecular ordering that occurs in condensed phases by studying a map of the structural order parameters (τ, Θ) for equilibrium and nonequilibrium packings in a simple system. Figure 9 represents such an *ordering phase diagram* constructed from molecular dynamics simulations of a collection of 500 identical hard spheres (Truskett *et al.*, 2000; Torquato *et al.*, 2000). Shown on the diagram are the equilibrium fluid, the equilibrium FCC crystal, and a set of glassy structures generated from the Lubachevsky–Stillinger compression protocol (Lubachevsky and Stillinger, 1990; Lubachevsky *et al.*, 1991). In this protocol, glassy hard-sphere packings are produced from low-density sphere configurations by allowing the hard-sphere diameter $\sigma(t)$ to grow linearly in time (at a given rate) during the course of a constant-volume molecular dynamics simulation. The compression protocol terminates when a high-density "jammed" sphere packing is achieved (Lubachevsky and Stillinger, 1990). As a result, the degree of disorder (as measured by τ and Θ) and the final packing fraction ϕ in the glasses depend on the "processing history" through the compression rate, i.e., the diameter growth rate.

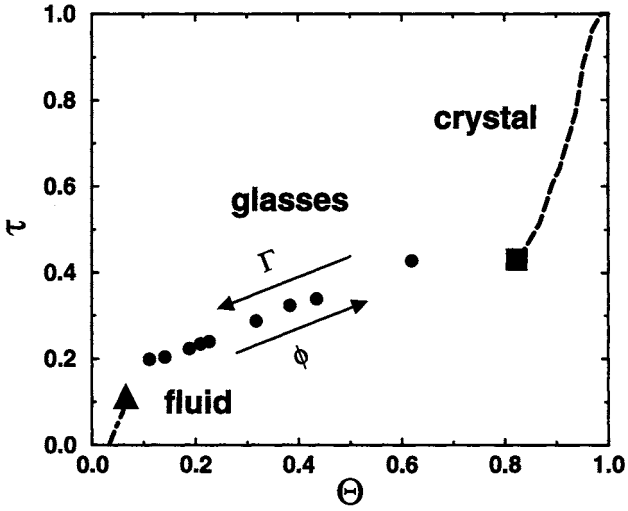

FIG. 9. Two-parameter ordering phase diagram for a system of 500 identical hard spheres (Truskett *et al.*, 2000; Torquato *et al.*, 2000). Shown are the coordinates in structural order parameter space (τ, Θ) for the equilibrium fluid (dot–dashed), the equilibrium FCC crystal (dashed), and a set of glasses (circles) produced with varying compression rates. Here, τ is the translational order parameter from (26) and Θ is the bond-orientational order parameter Q_6 from (25) normalized by its value in the perfect FCC crystal ($\Theta = Q_6/Q_6^{FCC}$). Each circle represents an average of 27 glasses produced by compressions at a given rate Γ. Unlike the equilibrium state points, the degree of ordering (τ, Θ) and the packing fraction ϕ in the glasses are determined by the processing history (in this case, the compression rate Γ). The freezing and melting transitions are indicated by the triangle and the square, respectively.

One striking feature of the ordering phase diagram shown in Fig. 9 is the strong positive correlation that exists between τ and Θ in the equilibrium hard-sphere fluid and crystalline phases. This indicates that entropy (i.e., packing efficiency) promotes an appreciable coupling between translational and bond-orientational order in the hard-sphere system. In addition, we note that there is a discontinuous jump in the structural order parameters across the first-order freezing transition, creating a large gap in order parameter space ($0.15 < \tau < 0.40$ and $0.1 < \Theta < 0.8$) that serves as a "no man's land" for the pure equilibrium phases. Interestingly, we find that sphere packings that exhibit an intermediate order, corresponding to coordinate pairs (τ, Θ) in no man's land, can be generated if we resort to a nonequilibrium (history-dependent) method for preparation, such as the Lubachevsky–Stillinger protocol. The observation that the jammed structures populate a different region of the ordering phase diagram than the equilibrium system indicates that certain nonequilibrium packings can be distinguished

statistically from the equilibrium configurations based on structural information alone. In particular, we note that the hard-sphere glasses are not simply solids with the "frozen-in" structure of the liquid.

Examination of the glassy sphere packings produced by the Lubachevsky–Stillinger protocol reveals that the amount of order in the structures can be statistically controlled by the compression rate. In fact, we note that "randomness" is a matter of degree in the jammed hard-sphere structures; i.e., jammed structures with slightly higher packing fractions ϕ can be realized at the expense of small increases in order (τ, Θ). This observation has recently led to a reassessment of the traditional notion that the random close-packed state is the densest possible amorphous sphere packing (Torquato *et al.*, 2000).

Although the ordering phase diagram presented in Fig. 9 was constructed from a highly idealized model system, it suggests challenging scientific questions about the morphology of real materials. For instance, it is clear that there exist large regions of the (τ, Θ) plane, i.e., certain types of molecular ordering, that are statistically inaccessible for a system in equilibrium. Is it possible to understand the relationship between these "inaccessible regions" in order parameter space and the relevant interactions in the system (i.e., the energy landscape)? In other words, can materials which possess a particular morphology be engineered by "tuning" their interactions? Moreover, can we use the ordering phase diagram as a viable guide for quantifying the relationship between disorder and history for realistic nonequilibrium protocols? Although we are far from answering these questions for real materials, the notion of an ordering phase diagram provides a useful conceptual framework for investigating the relationship among microscopic interactions, processing conditions, and the morphology of equilibrium and nonequilibrium systems.

The systematic investigation of order phase diagrams, such as that shown in Fig. 9 but for different molecular interactions, the location of inherent structures in the order plane, and the comparative exploration of order (or disorder) in "computer glasses" generated by different quenching protocols are, we believe, fruitful avenues for research into the nature, classification, and quantification of disorder in glasses and other technologically important nonequilibrium materials.

IV. Landscape Dynamics and Relaxation Phenomena

We presume in what follows that the supercooled liquid or glass of interest can be described by classical mechanics. Assuming that $\mathbf{r}_j$ comprises

Cartesian coordinates for all nuclei of particle j, the isochoric dynamical evolution of the N-particle system follows the Newtonian equations of motion:

$$\mathbf{m}_j \cdot d^2\mathbf{r}_j/dt^2 = -\nabla_j \Phi \qquad (1 \leq j \leq N). \tag{27}$$

The diagonal matrix $\mathbf{m}_j$ specifies the masses of the nuclei. Recall that Φ includes both intraparticle and interparticle potentials, as well as interactions of particles with confining walls that define system volume V. The qualitative nature of the trajectory traced out by the system configuration point,

$$\mathbf{R}(t) \equiv [\mathbf{r}_1(t), \mathbf{r}_2(t), \ldots, \mathbf{r}_N(t)], \tag{28}$$

as it evolves by Eqs. (27) depends strongly on the magnitude of the total energy. If that total energy is high, $\mathbf{R}(t)$ is able to move over the landscape with relatively little hindrance, moving quickly from basin to basin without being forced to pass close to the locations of basin-boundary saddle points. This situation typically describes liquids well above their melting temperatures. A variety of computer simulations (LaViolette and Stillinger, 1985a; Buchner *et al.*, 1992; Moore and Keyes, 1994; Wu and Tsay, 1996; La Nave *et al.*, 2000; Keyes, 1997; Keyes *et al.*, 1997) have established that $\mathbf{R}(t)$ in these high-energy circumstances moves across parts of the landscape at which the Hessian matrix (of second Φ derivatives) has a significant fraction of negative eigenvalues. In other words, the instantaneous normal mode (INM) spectrum for hot liquids exhibits a significant fraction of imaginary frequencies. Mode coupling theory (MCT) describes this situation well (Leutheusser, 1984; Bengtzelius *et al.*, 1984; Götze and Sjögren, 1992, 1995). In this high-temperature situation, a landscape-based description of liquid dynamics is not required, although still applicable in principle.

Lowering the total energy reduces the rate of interbasin transitions, obliges $\mathbf{R}(t)$ during those transitions to pass on average closer to the saddle points, and produces a reduction in the fraction of Hessian eigenvalues that are negative. As noted in Section II, the mean depth $\bar{\phi}$ of the basins visited by $\mathbf{R}(t)$ increases in absolute value as the energy and/or temperature decline, so that smaller and smaller subsets of basins can be visited. In the very low-energy/low-temperature range, interbasin transitions become very infrequent and, at least for solid amorphous materials, will be dominated by low-barrier transitions. These few remaining transitions are conventionally identified as two-level systems, and they have important consequences for heat capacity and sound propagation measurements on those amorphous solids (Phillips, 1972; Anderson *et al.*, 1972).

Whereas MCT appears well suited to describe dynamics and relaxation processes in liquids that are above, at, or moderately below their equilibrium melting points (Götze and Sjögren, 1995), it becomes physically inappropriate for strongly supercooled liquids and the glasses that they form

below an experimental (or simulational) glass transition temperature T_g. MCT erroneously predicts a singular temperature T_x below which the N-body system loses ergodicity, i.e., loses the ability to display complete relaxation to equilibrium (or restricted equilibrium for noncrystallizing liquids). One has

$$T_g < T_x \tag{29}$$

and typically T_x is 10 or 20% higher than T_g (Debenedetti, 1996). This shortcoming arises from the failure of the original MCT (Bengtzelius *et al.*, 1984) to incorporate landscape details and their profound influence on low temperature behavior. More recent elaborations of MCT (Sjögren and Götze, 1991; Götze and Sjögren, 1992) address this problem by incorporating a coupling between density and momentum fluctuations.

A few general observations are in order here about basin shapes and about the transitions that carry the system from one basin to a neighboring one. First, the intrabasin vibrational motions are substantially anharmonic for liquids at and slightly below their melting temperature T_m. One measure of this anharmonicity has already been mentioned, the incidence of negative eigenvalues of the Hessian matrix. Another revealing measure is the mean-square displacement of the configuration point, on a per-particle basis, from the inherent structure, plotted versus the temperature. This would be a straight line proportional to T if the basin interior were exactly harmonic, assuming classical statistics apply. However, as the schematic Fig. 10

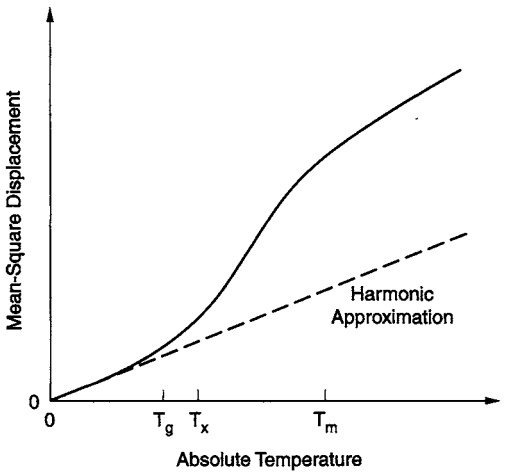

FIG. 10. Schematic illustration of mean-squared atomic displacements versus temperature, measured from the inherent structure, for amorphous-phase basins. The melting, MCT singular, and glass transition temperatures are T_m, T_x, and T_g, respectively.

indicates, the initial harmonic rise for low temperature becomes significantly enhanced at higher T due to strong anharmonicity (Sastry *et al.*, 1998a). This enhancement appears to arise from the contribution of basin "arms" that stretch outward from the inherent structure configuration, while rising only slowly in potential energy with distance (LaViolette and Stillinger, 1986). The anharmonic augmentation of the root-mean-square displacement is substantially larger for amorphous (liquid) basins than for crystalline basins, and this distinction has led to generalization of the venerable Lindemann melting criterion (Lindemann, 1910; Martin and O'Connor, 1977) to include a liquid freezing criterion (LaViolette and Sillinger, 1985a).

Computer simulations for several models (Weber and Stillinger, 1985; Ohmine, 1995) have determined that the elementary transitions between neighboring basins entail shifts of only small local groups of particles. To be precise, the difference between the inherent structures of the two basins involved in a large N-particle system is concentrated on a neighboring set of $O(1)$ particles; the remainder particles experience at most a minor elastic response to the localized repacking (Lacks, 1998). In view of the fact that the number of such localized repacking possibilities is proportional to system size, the number of transition states (saddle points) in the boundary of any basin will be $O(N)$, i.e., an extensive property. So too, then, will be the net kinetic exit rate from any basin at positive temperature.

It is important to bear in mind that the localized nature of the fundamental transitions implies that their respective saddle points lie only an $O(1)$ excitation energy above the bottom of the basin from which the system exits. In contrast, the total excitation energy possessed by the system while it resides in that basin will be an $O(N)$ quantity, even at very low temperatures. The central issue then becomes how long on average the system must wait before the intrabasin dynamics concentrates sufficient energy along the direction of the saddle point to permit the transition to the neighboring basin. This is the N-body analogue of the same issue that arises in chemical kinetics theory of unimolecular decomposition for variable intramolecular excitation energy (Gilbert and Smith, 1990).

At least in the temperature range relevant to liquid supercooling and glass formation, the kinetics of interbasin transitions and resulting relaxation phenomena can be described by a master equation (Stillinger, 1985). Suppose that the conserved system energy is E, and let $P_\alpha(t)$ stand for the probability that the system's configuration point resides in basin α at time t. The master equation takes the form

$$dP_\alpha(t)/dt = \sum_\gamma [K(\gamma \to \alpha|E)P_\gamma(t) - K(\alpha \to \gamma|E)P_\alpha(t)], \qquad (30)$$

where with obvious notation the K's are transition rates between neighboring basins α and γ at system energy E. These $O(1)$ rates are required to satisfy

detailed balance conditions to assure that Eq. (30) has time-independent equilibrium solutions. Specifically, for all α,γ pairs, the following equality must hold:

$$M_\alpha(E)K(\alpha \to \gamma|E) = M_\gamma(E)K(\gamma \to \alpha|E). \tag{31}$$

Here M_α and M_γ are the microcanonical measures of the interiors of basins α and γ at energy E. Equation (31) ensures that total probability is conserved at all times,

$$\sum_\alpha P_\alpha(t) = 1, \tag{32}$$

even when the system is out of equilibrium.

The general solution to the linear master equation (30) consists of a linear combination of eigenfunctions (equal in number to the number of basins that can be occupied):

$$P_\alpha(t) = \sum_{n\geq 0} A_n \chi_\alpha^{(n)}(E)\exp[-\lambda_n(E)t] \qquad (\lambda_n(E) \geq 0). \tag{33}$$

Initial conditions determine the linear combination coefficients A_n, which express the relative contribution of the nth eigenfunction. Thermal equilibrium at energy E corresponds to a vanishing decay constant, say λ_0, and in connection with earlier remarks, the collection of eigenfunctions $\chi_\alpha^{(0)}(E)$ is strongly concentrated in those basins whose depths are close to the $\bar{\phi}$ for the given E. The terms in expression (33), with $\lambda_n > 0$ $(n > 0)$ describe relaxation toward equilibrium.

A supercooled liquid or amorphous solid can be driven out of (restricted) equilibrium in a wide variety of ways, and the kinetics of relaxation back to (restricted) equilibrium subsequently followed. This variety includes sudden temperature or pressure changes, mechanical working, application of a polarizing electric field, and irradiation with energetic particles. As mentioned in Section I, the linear-response relaxation kinetics of supercooled liquids as monitored by any of several properties is observed to follow a Kohlrausch–Williams–Watts (KWW) stretched exponential form [see Eq. (2)],

$$f(t) = f(0)\exp\{-[t/\tau(T)]^{\beta(T)}\}, \tag{34}$$

where stretching exponent $\beta(T)$ empirically tends to fall in the range

$$\tfrac{1}{3} \leq \beta(T) \leq 1. \tag{35}$$

The relaxation time τ in Eq. (35) should not be confused with the

translational order parameter defined in Eq. (26). The mean relaxation time defined by $f(T)$ is

$$t_{\mathrm{rel}}(T) = \int_0^\infty tf(t)dt \Big/ \int_0^\infty f(t)dt = [\Gamma(2/\beta)/\Gamma(1/\beta)]\tau(T) \qquad (36)$$

The tendency is for $\beta(T)$ to decline with declining temperature, and as β passes downward between the limits shown in Eq. (35), the coefficient of τ in Eq. (36) increases from 1 to 60.

By expressing $f(t)$ as a Laplace transform,

$$f(t) = f(0)\int_0^\infty F(\lambda)\exp(-\lambda t)dt, \qquad (37)$$

the stretched exponential formally becomes resolved into individual simple-exponential decays with a range of decay rates. This allows contact with the general solution shown above in Eq. (33), with the understanding that for any property Q the observable relaxation would follow the form

$$Q(t) = \sum_\alpha Q_\alpha P_\alpha(t) = \sum_n \left(\sum_\alpha Q_\alpha A_n \chi_\alpha^{(n)} \right) \exp(-\lambda_n t) \cong \int_0^\infty q(\lambda)\exp(-\lambda t)d\lambda. \qquad (38)$$

Here Q_α is the mean value of property Q averaged over basin α (at energy E), and $q(\lambda)$ is the spectral weight in the continuum limit of the modes with exponential decay constant λ. If $Q(t)$ in fact has the stretched exponential form, then $q(\lambda)$ will be proportional to the Laplace transform $F(\lambda)$, for which both numerical (Lindsey and Patterson, 1980) and analytical (Helfand, 1983) studies are available. In the simple exponential decay limit $\beta = 1$, $F(\lambda)$ reduces to an infinitely narrow Dirac delta function but it broadens as β decreases toward the lower limit $\frac{1}{3}$ to involve a wide range of simple exponential relaxation rates.

An obvious question to ask is what characteristics of the basin distribution and of the kinetic connections between them can produce the wide spectrum of relaxation rates and the associated stretched exponentials. Some hints may come from simple models for supercooling and glass formation, whose kinetics are known to display stretched exponential relaxation functions. Two such models are the Fredrickson–Andersen kinetic Ising model (Fredrickson, 1984) and the tiling model (Weber *et al.*, 1986). Both involve discrete space rather than a continuum, and both view the glass-forming medium as residing in two dimensions rather than three. Nevertheless, these models indicate that as the temperature declines and as deeper and deeper portions of the respective (discrete) potential functions are probed, larger and larger clusters of "particles" must be rearranged for the system to find

yet lower potential energy configurations. Furthermore, increasing diversity arises in how these rearrangements can occur, in both size and shape of the affected local regions.

The shear viscosity $\eta(T)$ measures the rate at which a liquid can rearrange in response to an applied shear stress. As explained in Section I, the extent to which the temperature dependence of $\eta(T)$ conforms to, or deviates from, Arrhenius behavior,

$$\eta(T) = \eta_0 \exp(E_\eta / k_B T), \tag{39}$$

forms the basis of the "strong" vs "fragile" classification of glass formers (Angell, 1985). Here η_0 and the activation energy for viscous flow E_η are substance-specific, but temperature-independent, constants at a fixed volume.

Molten silica (SiO_2) is often considered the prototypical strong glass former (Angell, 1988). Its density is relatively constant in the supercooled range (<1700°C), and in that range the Arrhenius form (39) provides a good description for $\eta(T)$. A numerical fit for that viscosity leads to the results (Mackenzie, 1961)

$$\begin{aligned} \eta_0 &\cong 1.6 \times 10^{-13} \text{ P} \\ E_\eta &\cong 180 \text{ kcal/mol.} \end{aligned} \tag{40}$$

The latter stems from a local mechanism that rearranges the silica network structure and, presumably, involves breakage and reformation of Si–O chemical bonds.

The situation is quite different for glass formers at the fragile extreme. *o*-Terphenyl (OTP; $C_{18}H_{14}$) is a prototypical case and a favorite subject of experimental investigation (Fujara *et al.*, 1992; Cicerone and Ediger, 1993; Wang and Ediger, 1999). Plotting $\ln \eta$ vs $1/T$ produces a graph with a strong upward curvature (see Fig. 4), the slope of which defines a temperature-dependent effective activation energy (Greet and Turnbull 1967; Plazek *et al.*, 1994):

$$E_\eta^{(\text{eff})}(T) = \partial \ln \eta / \partial (1/T). \tag{41}$$

It has been pointed out (Greet and Turnbull, 1967) that this activation energy rises from approximately one-fourth of the heat of vaporization for the liquid above its melting point to approximately five times the heat of vaporization when the temperature is reduced to $T_g \approx -35$°C. This rise by a factor of 20 unambiguously testifies that the OTP energy landscape is strongly heterogeneous. The portions of that landscape accessed at high temperatures permit structural relaxation by surmounting low-energy barriers, presumably each step of which involves only rearranging slightly a small number of molecules. In contrast, the very large $E_\eta^{(\text{eff})}(T \cong T_g)$ can arise only by

cooperative rearrangement of a large number of molecules, perhaps in the range 20–100. Furthermore, such rearrangements are unlikely to consist of single elementary transitions between neighboring basins; to pass from one low-lying basin to one of equal or greater depth, it may be required to pass upward in landscape altitude (energy) through a long sequence of elementary transitions before descending far away to a suitably deep basin. The latter concept is supported by the very small effective preexponential factor for OTP near T_g (Plazek *et al.*, 1994),

$$\eta_0^{(\mathrm{eff})}(T \cong T_g) \cong 7 \times 10^{-68}\ \mathrm{P}, \tag{42}$$

reflecting a large activation entropy associated with the great diversity of transition pathways possible between a pair of separated deep basins.

Figure 11 attempts to provide a schematic illustration for the landscape topographic differences just discussed for the strong (SiO_2) and fragile (OTP) extremes. Of course, most glass-forming liquids fall between these extremes and should be thought of as interpolating the topographies illustrated. Figure 11 intends to illustrate only one symmetry sector. The strong case involves a single "metabasin" down into which the cooling liquid could configurationally trickle, surmounting barriers but encountering no substantial traps. The contrasting fragile case displays deep and widely separated traps, i.e., a diverse collection of metabasins in the same symmetry sector. The

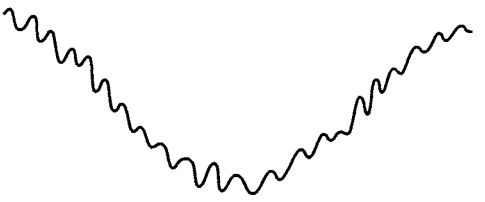

(a) Strong Glass Formers

(b) Fragile Glass Formers

FIG. 11. Schematic illustration of the topographic distinction between energy landscapes for strong and fragile glass formers. Only one symmetry sector is represented. Potential energy increases upward; the horizontal direction represents all configurational coordinates.

former, Fig. 11a, is similar to the configuration space "funnels" that have been postulated for properly folding biological proteins, while the latter, Fig. 11b, is characteristic of biologically useless misfolding proteins (Saven and Wolynes, 1997).

The long-pathway rearrangement processes expected for fragile materials at low temperatures are expected to be rare, to involve a local disruption of the otherwise well-structured amorphous medium, and to be relatively long-lived on the usual molecular time scale. These features all contribute to a substantial lengthening of the mean relaxation time $t_{rel}(T)$, Eq. (36), with declining temperature. Furthermore, the landscape diversity of deep traps and of the configuration space pathways that connect them should produce a broad spectrum of relaxation times, just as required by stretched-exponential relaxation functions, Eq. (34).

This scenario requires strongly supercooled fragile glass formers to be dynamically heterogeneous media, consisting at any instant mostly of nondiffusing well-bonded particles, but with a few local "hot spots" of mobile particles. The phenomenon of low-temperature dynamical heterogeneity has experimental support (Cicerone and Ediger, 1995) and has also been clearly documented by computer simulation (Donati *et al.*, 1999a,b; Bennemann *et al.*, 1999; Perera and Harrowell, 1996a,b). Both techniques confirm that the regions of anomalous mobility grow strongly in mean size with declining temperature.

The Stokes–Einstein relation connects shear viscosity η to the self-diffusion constant D in a liquid [see also Eq. (4)],

$$D(T) = k_B T/[6\pi a \eta(T)]. \tag{43}$$

For liquids composed of relatively compact molecules, this relation describes the temperature dependence of D well above the melting point and even for moderate supercooling, using the measured η and a temperature-independent a that tends to approximate roughly the size of the given molecular structure. However the Stokes–Einstein relation is based on macroscopic hydrodynamics that treats the liquid as a continuum. This hydrodynamic picture clearly contradicts the dynamic heterogeneity that applies to strongly supercooled fragile liquids. Perhaps, then, it should come as no surprise that the Stokes–Einstein relation fails dramatically in those circumstances: $D(T \cong T_g)$ has been observed experimentally to be 10^2 to 10^3 times larger than Eq. (43) predicts, retaining the same a that is applicable at high temperatures (Fujara *et al.*, 1992; Cicerone and Ediger, 1993; Kind *et al.*, 1992; Cicerone and Ediger, 1996). It has been pointed out (Stillinger and Hodgdon, 1994) that this D enhancement can arise from a suitable combination of mobile-region volume fraction, size, and lifetime.

No intrinsic mathematical reason exists to connect the depth distribution of the basins to the kinetic pathways between them. The latter depend

on the height of saddle points connecting neighboring basins. However, intermolecular interactions, particularly those for fragile glass formers, constitute a very special class of functions. Considerations similar to those that have suggested the form of Fig. 11b might also suggest that the rugged landscape obeys a statistical scaling relation. This is the basis of the formula suggested long ago by Adam and Gibbs (1965), which connects the kinetic property $t_{\rm rel}$ or, equivalently, η to supercooled liquid thermodynamics:

$$t_{\rm rel},\ \eta \cong A \exp(B/Ts_{\rm conf}). \tag{44}$$

Here A and B are positive constants, expected to depend on which of $t_{\rm rel}$ or η is involved, and $s_{\rm conf}$ is the molar configurational entropy to be obtained from calorimetric measurements for crystal, liquid, and glass. $s_{\rm conf}$ is a measure of the landscape's "ruggedness" and is related to the basin enumeration function introduced in Section II,[11]

$$s_{\rm conf}/R = \sigma_a[\bar{\phi}_a(T)], \tag{45}$$

where R is the gas constant. For Eq. (44) to hold, one must have

$$E_\eta^{\rm (eff)}(T) \propto 1/\sigma_a[\bar{\phi}_a(T)]; \tag{46}$$

that is, the effective dynamical excitation energy should be inversely proportional to the depth-dependent basin enumeration function σ_α evaluated at the depth populated at the given temperature. Thus, in the Adam–Gibbs picture, the origin of viscous slowdown close to $T_{\rm g}$ is the dearth of basins (configurations) that the system is able to sample at low temperatures. Furthermore, structural arrest is predicted to occur at the Kauzmann temperature. If the configurational entropy has the form[12] (Debenedetti, 1996; Richert and Angell, 1998),

$$s_{\rm conf} = s_\infty \left(1 - \frac{T_{\rm K}}{T}\right), \tag{47}$$

where $T_{\rm K}$ is the Kauzmann temperature (at which $s_{\rm conf}$ presumably vanishes), the Adam–Gibbs relation reads

$$\eta = A \exp\left(\frac{\tilde{B}}{T - T_{\rm K}}\right). \tag{48}$$

This is the VTF equation [see (1)], with T_0, the temperature of structural arrest, equal to $T_{\rm K}$. The remarkable closeness of these two temperatures for several substances [T_0 obtained from relaxation measurements and $T_{\rm K}$ from

[11] The experimental determination of the configurational entropy from calorimetric (heat capacity) measurements is discussed in Section V.

[12] Equation (47) results when the heat capacity difference between the supercooled liquid and the crystal is inversely proportional to the absolute temperature, as is experimentally found to be the case for many substances (Alba *et al.*, 1990).

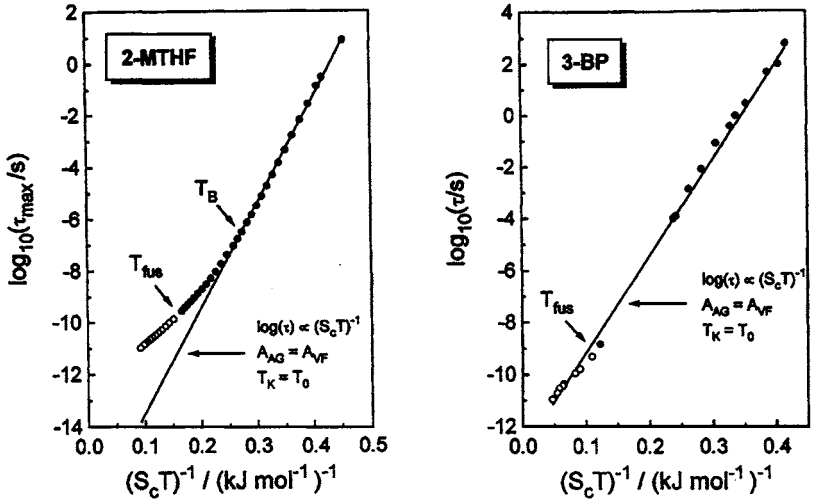

FIG. 12. Adam–Gibbs plots of the dielectric relaxation time of 2-methyltetrahydrofuran (2-MTHF) and 3-bromopentane (3-BP) versus $(Ts_{conf})^{-1}$. The lines are VTF fits, T_{fus} is the fusion temperature, and T_B is the temperature below which the VTF equation applies. A_{AG} and A_{VF} are prefactors in the Adam–Gibbs and VTF equations, respectively. T_K is the calorimetrically determined Kauzmann temperature, and T_0 is the VTF singular temperature, which were set equal in the VTF (line) fits. (Reprinted with permission from R. Richert and C. A. Angell. Dynamics of glass-forming liquids. V. On the link between molecular dynamics and configurational entropy. *J. Chem. Phys.* (1998); 108:9016. Copyright © 1998, American Institute of Physics.)

calorimetric experiments (Angell, 1997)] was mentioned in Section I. This is an example of the apparent connection between dynamics and thermodynamics in glasses (Wolynes, 1988). Figure 12 (Richert and Angell, 1998) shows the dielectric relaxation time for 2-methyltetrahydrofuran (MTHF) and 3-bromopentane (3-BP), plotted in Adam–Gibbs fashion. It can be seen that the theory provides an adequate description of the dielectric relaxation in 3-BP, but less so for MTHF. The Adam–Gibbs theory, in other words, is approximate and not general. Nevertheless, it remains a very useful and popular analytical framework for correlating and extrapolating data. Understanding the connection between kinetic properties and thermodynamics on which the Adam–Gibbs theory is based is arguably the most important problem in the thermophysics of glasses and supercooled liquids.

V. Thermodynamics

The statistical description of an energy landscape needed to make connection with thermodynamic properties is provided by the basin enumeration

function, $\sigma(\phi)$, introduced in Section II,

$$\frac{d\Omega}{d\phi} = C \exp[N\sigma(\phi)], \tag{11}$$

where $d\Omega$ is the number of potential energy minima whose depth, on a per-molecule basis, is $\phi \pm d\phi/2$; N is the number of molecules; and C is constant (Stillinger, 1999). It follows from the above equation that σ, the basin enumeration function, is the configurational entropy per molecule arising from the existence of multiple minima of depth ϕ [see also Eq. (45)],

$$\frac{S_{\text{conf}}}{Nk_{\text{B}}} = \sigma. \tag{49}$$

As explained in Section II, the partition function can be written as a one-dimensional integral over the basin depth ϕ (Stillinger and Weber, 1982). In the thermodynamic limit, the integral in Eq. (15) is dominated overwhelmingly by basin depths in the neighborhood of a particular, temperature-dependent value, which satisfies the extremum condition

$$\frac{\partial}{\partial\phi}(\sigma - \beta\phi - \beta a^{v}) = 0, \tag{50}$$

whereupon the Helmholtz energy can be written

$$-\beta A(\beta)/N = \sigma[\bar{\phi}(\beta)] - \beta\bar{\phi}(\beta) - \beta a^{v}[\beta, \bar{\phi}(\beta)]. \tag{16}$$

For the limiting case where a^{v} does not depend on ϕ (i.e., all basins have the same mean curvature at their respective minima), $\bar{\phi}$ follows from the condition

$$\frac{d\sigma}{d\phi} = \frac{1}{k_{\text{B}}T}. \tag{51}$$

Equation (16) establishes the formal connection between the thermodynamic properties of a system and its energy landscape. In particular, it expresses the Helmholtz energy in terms of an energy contribution, $\bar{\phi}$, arising from the sampling of basins of a particular, temperature-dependent depth; a configurational entropy contribution, σ, due to the existence of an exponential multiplicity of such basins [Eq. (11)]; and a vibrational contribution that arises from the thermal excitation that allows the system to sample basins at a temperature-dependent "height" above the local potential energy minimum.

The basin enumeration function $\sigma(\phi)$ can be obtained from experimental thermodynamic data. Because experiments are commonly done at constant pressure, Eqs. (13), (15), (16), and (50) must be recast in terms of the isobaric,

isothermal (N, P, T) ensemble. Following arguments identical to those in the isochoric case, the important result (Stillinger, 1998) is

$$-\beta G(\beta)/N = \sigma[\bar{\psi}(\beta)] - \beta\bar{\psi}(\beta) - \beta g^{\nu}[\beta, \bar{\psi}(\beta)], \tag{52}$$

where G is the Gibbs free energy, ψ is a "potential enthalpy" basin depth per particle [see also Eqs. (21) and (22)], and g^{ν} is the intrabasin vibrational Gibbs free energy per particle. To construct $\sigma(\psi)$, we consider the equilibrium between a liquid (l) and its crystal (x) at the melting point (T_m, P_m):

$$-\sigma^{(l)}(\bar{\psi}) + \beta_m\bar{\psi}^{(l)} + \beta_m g^{\nu}(\beta, \bar{\psi})^{(l)} = -\sigma^{(x)}(\bar{\psi}) + \beta_m\bar{\psi}^{(x)} + \beta_m g^{\nu}(\beta, \bar{\psi})^{(x)}. \tag{53}$$

Because the crystal is confined to a single basin, $\sigma^{(x)} = 0$. If the intrabasin vibrational free energy depends only on temperature, the above equation simplifies to

$$\sigma^{(l)} = \beta_m\left[\psi^{(l)} - \psi^{(x)}\right], \tag{54}$$

$\sigma^{(l)}$ corresponds to the entropy of fusion, and $\psi^{(l)} - \psi^{(x)}$ corresponds to the enthalpy of fusion. For $T < T_m$ and $P = P_m$, we can therefore write

$$\psi^{(l)}(\beta, P_m) - \psi^{(x)}(\beta, P_m) \equiv \Delta\psi = \Delta h_m - \int_T^{T_m} \Delta c_p dT \tag{55}$$

$$\sigma^{(l)}(\beta, P_m) = \frac{\Delta h_m}{k_B T_m} - \frac{1}{k_B}\int_T^{T_m} \frac{\Delta c_p}{T} dT, \tag{56}$$

where $\Delta c_p = c_p^{(l)} - c_p^{(x)}$. Thus, one can calculate the enthalpy excitation profile, $\psi^{(l)} - \psi^{(x)} = f_1(T)$, and the configurational entropy, $\sigma^{(l)} = f_2(T)$, from heat capacity data. Cross-plotting yields the desired basin enumeration function, $\sigma = \sigma(\Delta\psi)$ (Stillinger, 1998; Speedy, 1999). Equations (55) and (56) are valid under the assumption that the vibrational free energies of the crystal and the liquid are equal at the same temperature. Experimentally, this would result in negligible differences between crystalline and glassy heat capacities. Examples of such substances include OTP (Chang and Bestul, 1972) and 3-methylpentane (Takahara *et al.*, 1994). 1-Propanol, in contrast, shows nonnegligible differences between vitreous and crystalline heat capacities (Takahara *et al.*, 1994). These differences have not been taken into account in the calculations shown below.

Figure 13 shows the isobaric basin enumeration functions for 1-propanol and 3-methylpentane, at various pressures in the range 0–2 kbar. Figure 14 shows the corresponding excitation profiles. Figure 15 illustrates schematically the salient characteristics of the isobaric basin enumeration function.

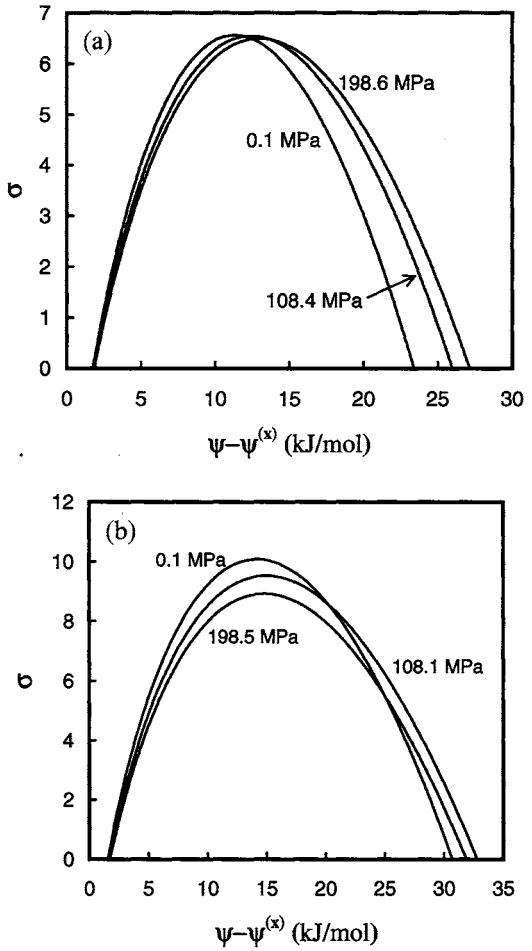

FIG. 13. Isobaric basin enumeration functions for 1-propanol (a) and 3-methylpentane (b) at different pressures. The x axis gives the difference between inherent structure and crystalline "potential enthalpies." Calculations performed according to Eqs. (55) and (56), using the experimental heat capacity data of Takahara *et al.* (1994). (From Lewis, 2000.)

The characteristic temperature-dependent basin depth is obtained from the condition [see also Eq. (51)]

$$\frac{d\sigma(\Delta\psi)}{d\Delta\psi} = \frac{1}{k_B T}. \tag{57}$$

Temperature increases monotonically from the point where $\sigma = 0$ ($d\sigma/d\Delta\psi > 0$ branch) to the top of the curve, which corresponds to the

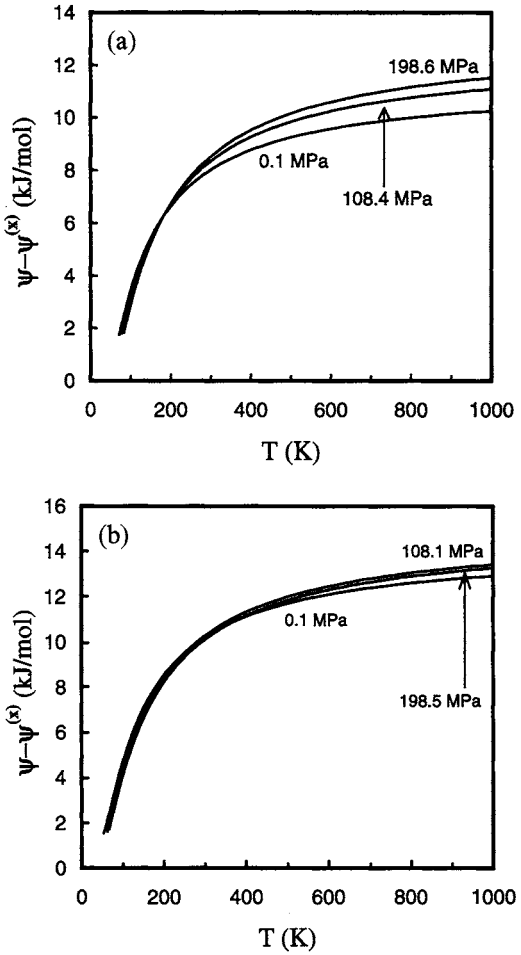

FIG. 14. Isobaric excitation profiles for 1-propanol (a) and 3-methylpentane (b) at different pressures. The y axis gives the "potential enthalpy" difference between the amorphous basin sampled preferentially at a given temperature and the single crystalline basin. Calculations performed according to Eq. (55), using the experimental heat capacity data of Takahara *et al.* (1994). (From Lewis, 2000.)

limit $T \to \infty$. The condition $\sigma = 0$ implies the existence of a unique basin; it therefore corresponds to the Kauzmann temperature T_K, where the entropy of the supercooled liquid equals that of the stable crystal.[13] When the system is in this unique basin, it has attained the lowest possible energy that a noncrystalline packing can adopt. This condition is called the ideal glass. The

[13] This is contingent on the assumption that $d\sigma/d\psi$ remains finite (see Stillinger, 1988).

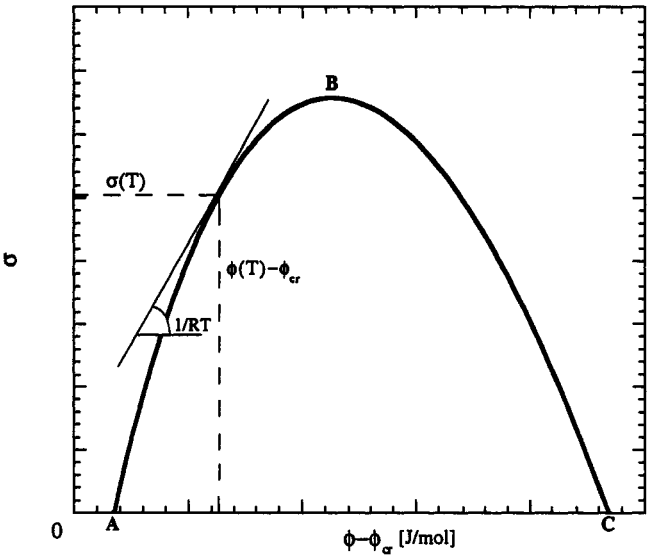

FIG. 15. Schematic isobaric basin enumeration function. Also shown is the graphical construction that yields σ and $\Delta\psi$ at each temperature. See also Eqs. (50) and (57). (From Lewis, 2000.)

negatively sloped portion of the basin enumeration function corresponds to negative temperatures and is therefore not physically relevant for the present purposes.

The similarity between the calculated isobaric excitation profiles shown in Fig. 14 and the isochoric profiles obtained by molecular simulation (Sastry *et al.*, 1998a) is remarkable. The isobaric excitation profiles have a discontinuity (not shown) at T_K: for $T < T_K$ the system remains trapped in the unique (ideal glass) basin, and $\Delta\psi$ is constant. The discontinuity is absent in the simulated isochoric profiles, because the system gets trapped kinetically in a cooling rate-dependent basin and is not able to access the deepest amorphous basin.

The approximately parabolic shape of the curves in Fig. 13 suggests the parametrization

$$\sigma = \sigma_\infty - m(\Delta\psi - \Delta\psi_\infty)^2, \tag{58}$$

where $\Delta\psi_\infty$ is the infinite temperature limit of $\Delta\psi$, and σ_∞ is the corresponding configurational entropy (Fig. 15). Table I (Lewis, 2000) gives the values of, σ_∞, m, and $\Delta\psi_\infty$ for 1-propanol and 3-methylpentane, as a function of pressure. The calculated isobaric basin enumeration functions are asymmetric, and Eq. (58) describes the curves accurately only if different values of m

TABLE I
GAUSSIAN LANDSCAPE PARAMETERS FOR 1-PROPANOL AND 3-METHYLPENTANE CALCULATED FROM HEAT CAPACITY MEASUREMENTS[a]

P (MPa)	σ_∞	$\Delta\psi_\infty$ (kJ/mol)	$100\,m$ (mol/kJ)^2
1-Propanol			
0.1	6.564	11.3	6.8
108.4	6.549	12.4	5.49
198.6	6.499	13.0	4.96
3-Methylpentane			
0.1	10.083	14.2	5.87
108.1	9.532	15.0	5.00
198.5	8.927	14.8	4.90

[a] From Takahara *et al.* (1994).

are used for positive and negative temperatures. Since only the former have physical significance, it seems prudent at this stage in our understanding of landscape statistics to preserve the simplicity of Eq. (58) rather than to include higher-order terms in an attempt to capture the slightly asymmetric character of the basin enumeration function. Landscapes with parabolic enumeration functions will henceforth be referred to as *Gaussian* (Speedy, 1999; Büchner and Heuer, 1999).

Several useful relations can be written for systems with Gaussian landscapes. The excitation profile satisfies the relation

$$\Delta\psi = \begin{cases} \Delta\psi_\infty - \dfrac{1}{2mk_BT} & (T > T_K) \\ \Delta\psi_\infty - \dfrac{1}{2mk_BT_K} & (T \le T_K). \end{cases} \tag{59}$$

Combining Eqs. (16), (51), and the isochoric analogue of (58),

$$\sigma = \sigma_\infty - m(\phi - \phi_\infty)^2, \tag{60}$$

leads to the following expression for the Helmholtz free energy:

$$-\beta A/N = \sigma_\infty + \beta\phi_\infty - \beta^2/4m - \beta a^v. \tag{61}$$

The equation of state follows by differentiation,

$$\beta P/\rho = \beta\frac{d\phi_\infty}{d\ln\rho} - \frac{d\sigma_\infty}{d\ln\rho} + \left(\frac{\beta}{2m}\right)^2\frac{dm}{d\ln\rho} + \left(\frac{\partial\beta a^v}{\partial\ln\rho}\right)_\beta. \tag{62}$$

Thus, all thermodynamic (equilibrium) properties of a macroscopic system with a Gaussian landscape can be calculated from knowledge of $\phi_\infty(\rho)$ (the density dependence of the basin depth per particle in the high-temperature limit), $\sigma_\infty(\rho)$ (the density dependence of the configurational entropy

associated with the existence of an exponential multiplicity of basins of a given depth, in the high-temperature limit), $m(\rho)$ (the density dependence of the effective width of the basin distribution), and $a^{\nu}(\beta, \rho)$ (the temperature and density dependence of the vibrational free energy). $\phi_{\infty}(\rho)$ and $m(\rho)$ can be obtained from molecular simulation studies that combine energy minimization and standard particle moves (e.g., Sastry *et al.*, 1998a; Jonsson and Andersen, 1988). Fitting the resulting excitation profiles to the isochoric analogue of Eq. (59) ($T > T_K$) yields ϕ_{∞} and m. The vibrational free energy can be obtained from the equation

$$A^{\nu} = \sum_{i=1}^{\nu N} \left[\frac{\hbar\omega_i}{2} + k_B T \ln\left(1 - e^{-\beta\hbar\omega_i}\right) \right], \tag{63}$$

where $\hbar$ is Planck's constant divided by 2π, ω_i are the density-dependent normal mode angular frequencies, and ν is the number of degrees of freedom per molecule[14] (Landau and Lifshitz, 1980). The normal mode frequencies are obtained from the Hessian matrix of second derivatives of the energy. For a Gaussian landscape,

$$\sigma_{\infty} = m\left(\phi_K - \phi_{\infty}\right)^2, \tag{64}$$

where ϕ_K corresponds to the deepest amorphous basin, that is, to the ideal glass. Thus, σ_{∞} can, in principle, be obtained numerically by performing a constrained optimization in which stable packings whose measures of order exceed a specified cutoff are excluded from consideration.

From the preceding discussion it can be concluded that significant progress in understanding the thermodynamics of complex condensed systems under conditions such that each constituent unit (for example, a molecule in the case of a molecular glass former or an amino acid residue in the case of a protein) experiences simultaneous strong interactions with many neighbors can result from a numerical investigation of basic landscape features (ϕ_{∞}, σ_{∞}, m) as a function of the density and molecular architecture. Recent studies by Sciortino *et al.* (1999) and by Büchner and Heuer (1999) demonstrate the powerful insights that can be gained by this approach.

The energy landscape perspective provides fresh insight into, and suggests unexpected connections between, stretched liquids and the glassy state. As shown in Fig. 8, the $p(\rho)$ relationship for mechanically stable packings of simple, atomic systems shown van der Waals-type behavior. We refer to this type of curve as the equation of state of an energy landscape (Debenedetti *et al.*, 1999). The landscapes of ethane, *n*-pentane, and cyclopentane exhibit similar behavior (Utz *et al.*, 2001). Water's landscape, in contrast, consists

[14] Equation (63) involves a proper quantum treatment of harmonic vibrational degrees of freedom.

of a family of $p(\rho)$ curves which depend on the temperature of the equilibrated liquid from which the energy minimization is performed (Roberts *et al.,* 1999). While our present understanding of those features of molecular architecture and interactions that give rise to a temperature-dependent landscape equation of state is far from complete, it is clear that orientation-dependent interactions are sufficient to cause this type of complexity. In what follows we restrict our attention to "simple," that is, temperature-independent, landscape equations of state.

The minimum in the $p(\rho)$ curve corresponds to the maximum tensile strength of which the amorphous form of a given material is capable. As mentioned in Section III, the density at which this occurs is called the Sastry density, an important material characteristic. Below the Sastry density, mechanically stable packings are fissured due to the appearance of large cavities (Sastry *et al.,* 1997b). Thus, this density is a limiting condition, below which amorphous packings can no longer be mechanically stable (i.e., minimum energy) and simultaneously spatially homogeneous. Since a glass is a liquid trapped in a mechanically stable configuration (potential energy minimum), it is not possible to form a homogeneous glass below a material's Sastry density.

The nonmonotonic shape of the $p(\rho)$ curve is reminiscent of the behavior of approximate equations of state, such as the van der Waals equation. It must be understood, however, that whereas the unstable portion of such equations is unphysical, the landscape equation of state is exact. Neighboring states on this curve, however, are not connected by a continuum of thermally equilibrated states. Rather, thermal motion having been removed by construction, the path from one point to another along the landscape equation of state is through the high-temperature equilibrated fluid. This caveat notwithstanding, there appears to be a deep and illuminating relationship between the spinodal curve for the superheated liquid and the Sastry point. The theoretical maximum for the tensile strength of noncrystalline forms of a material is given by the $T = 0$ limit of the spinodal curve along the superheated liquid branch (Debenedetti, 1996). Table II lists the predictions for the Sastry density ρ_s and maximum tensile strength P_s (i.e., the Sastry point), according to three cubic equations of state, and compares these theoretical predictions with our simulation results for the Lennard–Jones fluid (Fig. 8). Of course, none of these equations are accurate representations of the Lennard–Jones fluid. Nevertheless, the clear implication from the simulations is that the Sastry point corresponds to the $T = 0$ limit of the superheated liquid spinodal.

Since the Sastry density is an absolute (thermodynamic) limit to vitrification as $T \to 0$, it follows that the point (ρ_s, $T = 0$) is the low-temperature termination of the Kauzmann curve. Since materials are vitrified by cooling and/or compression, the Kauzmann curve is expected to have a positive slope

TABLE II
COMPARISON OF THEORETICAL PREDICTIONS OF THE SASTRY POINT (ρ_s, P_s) ACCORDING TO CUBIC EQUATIONS OF STATE AND SIMULATIONS[a]

	ρ_s/ρ_c	P_s/P_c
van der Waals	3	−27
Soave–Redlich–Kwong[b,c]	3.85	−62.5
Peng–Robinson[c,d]	3.95	−71.5
Simulation[e]	2.76	−39.8

[a] Subscript c denotes the value of a property at the critical point.
[b] From Soave (1972).
[c] An acentric factor $\omega = 0.001$ was used, corresponding to Ar (Reid *et al.*, 1987).
[d] From Peng and Robinson (1976).
[e] Smoothly truncated Lennard–Jones fluid (Sastry *et al.*, 1997b). See Fig. 8.

in the (T, ρ) plane. Our results suggest, therefore, that the low-temperature termination of the Kauzmann curve coincides with the $T \to 0$ limit of the superheated liquid spinodal.[15] The predicted convergence of two such apparently unrelated limits is surprising. It is not obvious why the limit of stability for the superheated liquid should tend to the locus along which the entropies of a deeply supercooled liquid and of its stable crystalline form coincide. Nevertheless, this conclusion from our simulations is supported by mean-field theoretical calculations (Debenedetti *et al.*, 1999). Figure 16 shows the calculated phase diagram of a soft-sphere system whose constituent atoms interact via a pairwise-additive spherically symmetric potential that decays as the inverse ninth power of the interatomic distance, plus a mean-field, van der Waals-type attraction. In addition to the phase coexistence loci, the diagram shows the Kauzmann curve, as well as the spinodal curves corresponding to the liquid–vapor transition. The remarkable feature of the calculation is the low-temperature convergence of the superheated liquid spinodal and the Kauzmann curve. Similar results have also been obtained for the hard-sphere and hard-dumbbell models with mean-field attraction.

In spite of the remarkable agreement between theoretical predictions, on the one hand, and the logical consequence of the simulations, on the other, we believe that the generality of behavior such as shown in Fig. 16 cannot be accepted uncritically but should instead be regarded as a fundamental open question on the properties of disordered materials. This caution is warranted by the approximate, mean-field nature of the calculations, as well as by microscopic critiques of the very notion of a Kauzmann temperature (Stillinger, 1988). Perhaps more significantly, recent experiments on

[15] For a contrasting viewpoint, see Sastry (2000).

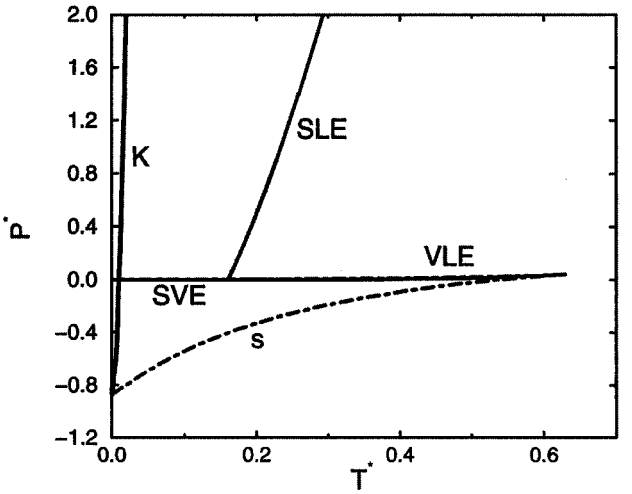

FIG. 16. Calculated phase diagram of the r^{-9} soft-sphere plus mean-field model, showing the vapor–liquid (VLE), solid–liquid (SLE), and solid–vapor (SVE) coexistence loci, the superheated liquid spinodal (s), and the Kauzmann locus (K) in the pressure–temperature plane ($P^* = P\sigma^3/\varepsilon; T^* = k_B T/\varepsilon$). The Kauzmann locus gives the pressure-dependent temperature at which the entropies of the supercooled liquid and the stable crystal are equal. Note the convergence of the Kauzmann and spinodal loci at $T = 0$. See Debenedetti *et al.* (1999) for details of this calculation.

poly(4-methylphentene-1), which show inverse melting at low temperatures and high pressures, that is, freezing upon heating, call into question the notion of an ideal glass and of the Kauzmann temperature as an absolute limit to supercooling (Rastogi *et al.*, 1999; Greer, 2000).

VI. Conclusion

In glasses and the supercooled liquids from which they are commonly formed, molecules are subject to the simultaneous action of many neighbors. Under these conditions the multidimensional N-body potential energy function $\Phi(\mathbf{r}_1 \ldots \mathbf{r}_N)$, the energy landscape, provides a convenient framework within which to describe the thermophysical properties of this important class of condensed-phase systems. Melting and freezing phenomena (LaViolette and Stillinger, 1985a), complex dynamics in supercooled liquids (Sastry *et al.*, 1998a), the mechanical strength of glasses (Utz *et al.*, 2001; Malandro and Lacks, 1997, 1999), the limits of stability of the liquid state of matter (Debenedetti *et al.*, 1999; Sastry, 2000), and aging phenomena in glasses (Utz *et al.*, 2000; Kob *et al.*, 2000) are some of the important phenomena on which the landscape perspective has yielded useful new insights.

Major open questions where landscape-based ideas should prove helpful include the possible thermodynamic basis for the glass transition (Debenedetti *et al.,* 1999), the relationship between kinetics and thermodynamics of deeply supercooled liquids and glasses (Adam and Gibbs, 1965; Wolynes, 1988), and translation–rotation decoupling and the breakdown of the Stokes–Einstein relationship in supercooled liquids (Fujara *et al.,* 1992). In addition, the reformulation of the thermodynamics of liquids embodied in Eqs. (16), (52), (55), (56), (61), and (62) suggests that understanding basic topological features of a landscape's density-dependent statistics could lead to improved theories of simple and complex liquids. As explained in Section V, landscape statistics can be obtained from experiments, theory, and simulations.

The quantitative description of disorder in liquids and glasses is the second theme of this article. Recent work on the simple hard-sphere system (Torquato *et al.,* 2000; Truskett *et al.,* 2000) shows that it is possible to distinguish equilibrium and nonequilibrium states based on the accessible types of molecular disorder. It is also possible to relate the type of molecular disorder to a glass' processing history. Extending these developments to models with more realistic interactions, and mapping their order phase diagrams, including their inherent structures, are some of the important questions, the answers to which could shed new light on the relationship among molecular interactions, process conditions, and the morphology of glasses. More generally, the problem of quantifying disorder in condensed phases has implications for early detection of tumors, transdermal drug delivery, flow through porous media, and powder engineering.

Glasses are central to a wide variety of commercial processes and technical applications, such as the preservation of labile biochemicals, food processing, the manufacture of optical wave guides, corrosion resistance, photovoltaic cells, and the extrusion and molding of engineering plastics. In spite of their widespread natural occurrence and technical utilization, there are major gaps in the present understanding of the vitreous state of matter. In this article we have presented a geometric viewpoint of glass transition phenomena and supercooling. These ideas have contributed significantly to contemporary knowledge of this important topic. We believe that they are likely to prove equally fruitful in the future.

ACKNOWLEDGMENTS

P.G.D. gratefully acknowledges the support of the U.S. Department of Energy, Division of Chemical Sciences, Geosciences, and Biosciences, Office of Basic Energy Science (Grant DE-FG02-87ER13714). T.M.T. acknowledges the support of the National Science Foundation.

REFERENCES

Abkevich, V. I., Gutin, A. M., and Shakhnovich, E. I., Free energy landscape for protein folding kinetics: Intermediates, traps, and multiple pathways in theory and lattice model simulations. *J. Chem. Phys.* **101,** 6052 (1994).

Adam, G., and Gibbs, J. H., On the temperature dependence of cooperative relaxation properties in glass-forming liquids. *J. Chem. Phys.* **43,** 139 (1965).

Alba, C., Busse, L. E., List, D. J., and Angell, C. A., Thermodynamic aspects of the vitrification of toluene and xylene isomers, and the fragility of light hydrocarbons. *J. Chem. Phys.* **92,** 617 (1990).

Anderson, P. W., Halperin, B. J., and Varma, C. M., Anomalous low-temperature properties of glasses and spin glasses. *Philos. Mag.* **25,** 1 (1972).

Angell, C. A., Strong and fragile liquids. *In* "Relaxations in Complex Systems" (K. Ngai and G. B. Wright, Eds.), Nat. Tech. Info. Ser., U.S. Dept. Commerce, Springfield, VA, 1985, p. 1.

Angell, C. A., Structural instability and relaxation in liquid and glassy phases near the fragile liquid limit. *J. Non-Cryst. Sol.* **102,** 205 (1988).

Angell, C. A., Formation of glasses from liquids and biopolymers. *Science* **267,** 1924 (1995).

Angell, C. A., Landscapes with megabasins: Polyamorphism in liquids and biopolymers and the role of nucleation in folding and folding diseases. *Physica D* **107,** 122 (1997).

Angell, C. A., and Kanno, H., Density maxima in high-pressure supercooled water and liquid silicon dioxide. *Science* **193,** 1121 (1976).

Angell, C. A., Clarke, J. H. R., and Woodcock, L. V., Interaction potentials and glass formation: A survey of computer experiments. *Adv. Chem. Phys.* **48,** 397 (1981).

Angell, C. A., Ngai, K. L., McKenna, G. B., McMillan, P. F., and Martin, S. W., Relaxation in glassforming liquids and amorphous solids. *J. Appl. Phys.* **88,** 3113 (2000).

Ashcroft, N. W., and Mermin, N. D., "Solid State Physics." Saunders College, Philadelphia, 1976.

Becker, O. M., and Karplus, M., The topology of multidimensional potential energy surfaces: Theory and application to peptide structure and kinetics. *J. Chem. Phys.* **106,** 1495 (1997).

Bengtzelius, U., Götze, W., and Sjölander, A., Dynamics of supercooled liquids and the glass transition. *J. Phys. C Sol. State Phys.* **17,** 5915 (1984).

Bennemann, C., Donati, C., Baschnagel, J., and Glotzer, S. C., Growing range of correlated motion in a polymer melt on cooling towards the glass transition. *Nature* **399,** 246 (1999).

Blanshard, J. M. V., and Lillford, P. J. (Eds.), "The Glassy State in Foods." Nottingham University Press, 1993.

Bowles, R. K., and Corti, D. S., Statistical geometry of hard sphere systems: Exact relations for first-order phase transitions in multicomponent systems. *Mol. Phys.* **98,** 429 (2000).

Brinon, L., Geiger, S., Alard, V., Doucet, J., Tranchant, J.-F., and Courraze, G., Percutaneous absorption of sunscreens from liquid crystalline phases. *J. Contr. Rel.* **60,** 67 (1999).

Brostow, W., Chybicki, M., Laskowski, R., and Rybicki, J., Voronoi polyhedra and Delaunay simplexes in the structural analysis of molecular-dynamics-simulated materials. *Phys. Rev. B* **57,** 13448 (1998).

Brüning, R., and Samwer, K., Glass transition on long time scales. *Phys. Rev. B* **46,** 318 (1992).

Bryant, S., and Blunt, M., Prediction of relative permeability in simple porous-media. *Phs. Rev. A* **46,** 2004 (1992).

Büchner, S., and Heuer, A., Potential energy landscape of a model glass former: Thermodynamics, anharmonicities, and finite size effects. *Phys. Rev. E* **60,** 6507 (1999).

Buchner, M., Ladanyi, B. M., and Stratt, R. M., The short-time dynamics of molecular liquids. Instantaneous-normal-mode theory. *J. Chem. Phys.* **97,** 8522 (1992).

Chan, H. S., and Dill, K. A., Transition-states and folding dynamics of proteins and heteropolymers. *J. Chem. Phys.* **100,** 9238 (1994).

Chang, S. S., and Bestul, A. B., Heat capacity and thermodynamic properties of o-terphenyl crystal, glass, and liquid. *J. Chem. Phys.* **56,** 503 (1972).

Chaudhari, P., and Turnbull, D., Structure and properties of metallic glasses. *Science* **199,** 11 (1978).

Cicerone, M. T., and Ediger, M. D., Photobleaching technique for measuring ultraslow reorientation near and below the glass transition—Tetracene in o-terphenyl. *J. Phys. Chem.* **97,** 10489 (1993).

Cicerone, M. T., and Ediger, M. D., Relaxation of spatially heterogeneous dynamic domains in supercooled ortho-terphenyl. *J. Chem. Phys.* **103,** 5684 (1995).

Cicerone, M. T., and Ediger, M. D., Enhanced translation of probe molecules in supercooled o-terphenyl: Signature of spatially heterogeneous dynamics? *J. Chem. Phys.* **104,** 7210 (1996).

Cusack, N. E., "The Physics of Structurally Disordered Matter: An Introduction." Adam Hilger, Bristol, 1987.

Davidson, D. W., *In* "Water, a Comprehensive Treatise" (Franks, F., Ed.), Vol. 2, Chap. 3. Plenum Press, New York, 1973.

Davis, H. T., "Statistical Mechanics of Phases, Interfaces, and Thin Films." VCH, New York, 1996.

Debenedetti, P. G., "Metastable Liquids," Princeton University Press. Princeton, NJ, 1996.

Debenedetti, P. G., Stillinger, F. H., Truskett, T. M., and Roberts, C. J., The equation of state of an energy landscape. *J. Phys. Chem. B* **103,** 7390 (1999).

Deem, M. W., Recent contributions of statistical mechanics in chemical engineering. *AIChE J.* **44,** 2569 (1998).

Dill, K. A., and Chan, H. S., From Levinthal to pathways and funnels. *Nature Struct. Biol.* **4,** 10 (1997).

Dodd, L. R., and Theodorou, D. N., Analytical treatment of the volume and surface area of molecules formed by an arbitrary collection of unequal spheres intersected by planes. *Macromolecules* **72,** 1313 (1991).

Donati, C., Glotzer, S. C., and Poole, P. H., Growing spatial correlations of particle displacements in a simulated liquid on cooling toward the glass transition. *Phys. Rev. Lett.* **82,** 5064 (1999a).

Donati, C., Glotzer, S. C., Poole, P. H., Kob, W., and Plimpton, S. J., Spatial correlations of mobility and immobility in a glass-forming Lennard–Jones liquid. *Phys. Rev. E* **60,** 3107 (1999b).

Ediger, M. D., Spatially heterogeneous dynamics in supercooled liquids. *Annu. Rev. Phys. Chem.* **51,** 99 (2000).

Ediger, M. D., Angell, C. A., and Nagel, S. R., Supercooled liquids and glasses. *J. Phys. Chem.* **100,** 13200 (1996).

Eisenberg, D., and Kauzmann, W., "The Structure and Properties of Water." Oxford University Press, New York, 1969, Chap. 3.

Errington, J. R., Unpublished results (2000).

Errington, J. R., and Debenedetti, P. G., Relationship between structural order and the anomalies of liquid water. *Nature,* **409,** 318 (2001).

Franks, F., Long-term stabilization of biologicals. *Biotechnology* **12,** 253 (1994).

Frauenfelder, H., and Wolynes, P. G., Biomolecules: Where the physics of complexity and simplicity meet. *Phys. Today* **Feb.,** 58 (1994).

Frauenfelder, H., Sligar, S. G., and Wolynes, P. G., The energy landscapes and motions of proteins. *Science* **254,** 1598 (1991).

Frauenfelder, H., Bishop, A. R., Garcia, A., Perelson, A., Schuster, P., Sherrington, D., and Swart, P. J. (eds.), Landscape paradigms in physics and biology. Concepts, structures and dynamics. *Physica D* **107,** Nos. 2–4 (1997).

Fredrickson, G. H., Linear and nonlinear experiments for a spin model with cooperative dynamics. *Ann. N.Y. Acad. Sci.* **484,** 185 (1986).

Frenkel, J., "Kinetic Theory of Liquids." Dover, New York, 1955, p. 174.

Fricke, J. (Ed.), "Aerogels." Spinger, Heidelberg, 1986.

Fujara, F., Geil, B., Sillescu, H., and Fleischer, G., Translational and rotational diffusion in supercooled orthoterphenyl close to the glass transition. *Z. Phys. B Cond. Matter* **88,** 195 (1992).

Fulcher, G. S., Analysis of recent measurements of the viscosity of glasses. *J. Am. Ceram. Soc.* **8,** 339 (1925).

Gibbs, J. H., and DiMarzio, E. A., Nature of the glass transition and the glassy state. *J. Chem. Phys.* **28,** 373 (1958).

Gilbert, R. J., and Smith, S. C., "Theory of Unimolecular and Recombination Reactions." Blackwell Scientific, Oxford, 1990.

Goldstein, M., On the temperature dependence of cooperative relaxation properties in glass-forming liquids—Comment on a paper by Adam and Gibbs. *J. Chem. Phys.* **43,** 1852 (1965).

Goldstein, M., Viscous liquids and the glass transition: A potential energy barrier picture. *J. Chem. Phys.* **51,** 3728 (1969).

Götze, W., and Sjögren, L., Relaxation processes in supercooled liquids. *Rep. Prog. Phys.* **55,** 241 (1992).

Götze, W., and Sjögren, L., The mode coupling theory of structural relaxations. *Transp. Theory Stat. Phys.* **24,** 801 (1995).

Greenfield, M. L., and Theodorou, D. N., Geometric analysis of diffusion pathways in glassy and melt atactic polypropylene. *Macromolecules* **26,** 4561 (1993).

Greer, A. L., Metallic glasses. *Science* **267,** 1947 (1995).

Greer, A. L., Too hot to melt. *Nature* **404,** 134 (2000).

Greet, R. J., and Turnbull, D., Glass transition in o-terphenyl. *J. Chem. Phys.* **46,** 1243 (1967).

Gubbins, K. E., and Quirke, N. (Eds.), "Molecular Simulation and Industrial Applications: Methods, Examples, and Prospects." Gordon and Breach, Amsterdam, 1996.

Guggenheim, E. A., "Thermodynamics," 2nd ed., Interscience, New York, 1950, p. 131.

Hama, Y., Suzuki, K., Shingu, K., Fujimori, M., Kobayashi, S., Usuda, N., and Amano, J., *Thyroid* **9,** 927 (1999).

Helfand, E., On inversion of the Williams-Watts function for large relaxation times. *J. Chem. Phys.* **78,** 1931 (1983).

Hinze, G., Francis, R. S., and Fayer, M. D., Translational-rotational coupling in supercooled liquids: Heterodyne detected density induced molecular alignment. *J. Chem. Phys.* **111,** 2710 (1999).

Hirschfelder, J. O., Curtiss, C. F., and Bird, R. B., "Molecular Theory of Gases and Liquids," John Wiley and Sons, New York, 1954, p. 250.

Huitema, H. E. A., Vlot, M. J., and van der Eerden, J. P., Simulations of crystal growth from Lennard–Jones melt: Detailed measurements of the interface structure. *J. Chem. Phys.* **111,** 4714 (1999).

Hurley, M. M., and Harrowell, P., Non-gaussian behavior and the dynamical complexity of particle motion in a dense two-dimensional liquid. *J. Chem. Phys.* **105,** 10521 (1996).

Hyde, P. D., Evert, T. E., and Ediger, M. D., Nanosecond and microsecond study of probe reorientation in orthoterphenyl. *J. Chem. Phys.* **93,** 2274 (1990).

Ito, K., Moynihan, C. T., and Angell, C. A., Thermodynamic determination of fragility in liquids and a fragile-to-strong liquid transition in water. *Nature* **398,** 492 (1999).

Jonsson, H., and Andersen, H. C., Icosahedral ordering in the Lennard-Jones crystal and glass. *Phys. Rev. Lett.* **60,** 2295 (1988).

Kauzmann, W., The nature of the glassy state and the behavior of liquids at low temperatures. *Chem. Rev.* **43,** 219 (1948).

Keyes, T., Instantaneous normal mode approach to liquid state dynamics. *J. Phys. Chem. A* **101,** 2921 (1997).

Keyes, T., Dependence of supercooled liquid dynamics on elevation in the energy landscape. *Phys. Rev. E* **59,** 3207 (1999).

Keyes, T., Vijayadamodar, G. V., and Zurcher, U., An instantaneous normal mode description of relaxation in supercooled liquids. *J. Chem. Phys.* **106,** 4651 (1997).

Kieffer, J., and Angell, C. A., Generation of fractal structures by negative pressure rupturing of SiO_2 glass. *J. Non-Cryst. Sol.* **106,** 336 (1988).

Kind, R., Liechti, O., Korner, N., Hulliger, J., Dolinsek, J., and Blinc, R., Deuteron-magnetic-resonance study of the cluster formation in the liquid and supercooled-liquid state of 2-cyclooctylamino-5-nitropyridine. *Phys. Rev. B* **45,** 7697 (1992).

Kittel, C., "Introduction to Solid State Physics," 7th ed., Wiley, New York, 1966.

Kob, W., Sciortino, F., and Tartaglia, P., Aging as dynamics in configuration space. *Europhys. Lett.* **49,** 590 (2000).

Kohlrausch, R., Theorie des elektrischen rückstandes in der leidener flasche. *Ann. Phys. Chem. (Leipzig)* **91,** 179 (1874).

Lacks, D. J., Localized mechanical instabilities and structural transformations in silica glass under high pressure. *Phys. Rev. Lett.* **80,** 5385 (1998).

Lacks, D. J., and Wienhoff, J. R., Disappearences of energy minima and loss of order in polydisperse colloidal systems. *J. Chem. Phys.* **111,** 398 (1999).

LaNave, E., Scala, A., Starr, F. W., Sciortino, F., and Stanley, H. E., Instantaneous normal mode analysis of supercooled water. *Phys. Rev. Lett.* **84,** 4605 (2000).

Landau, L. D., and Lifshitz, E. M., "Statistical Physics. Part 1," Vol. 5 of Course on Theoretical Physics. 3rd ed., Chap. 6, Pergamon Press, Oxford, 1980.

Laughlin, R. B., Pines, D., Schmalian, J., Stojkovic, B. P., and Wolynes, P., The middle way. *Proc. Natl. Acad. Sci. USA* **97,** 32 (2000).

Laughlin, W. T., and Uhlmann, D. R., Viscous flow in simple organic liquids. *J. Phys. Chem.* **76,** 2317 (1972).

LaViolette, R. A., Amorphous deposits with energies below the crystal energy. *Phys. Rev. B* **40,** 9952 (1989).

LaViolette, R. A., and Stillinger, F. H., Multidimensional geometric aspects of the solid-liquid transition in simple substances. *J. Chem. Phys.* **83,** 4079 (1985a).

LaViolette, R. A., and Stillinger, F. H., Consequences of the balance between the repulsive and attractive forces in dense, non-associated liquids. *J. Chem. Phys.* **82,** 3335 (1985b).

LaViolette, R. A., and Stillinger, F. H., Thermal disruption of the inherent structure of simple liquids. *J. Chem. Phys.* **85,** 6027 (1986).

Leutheusser, E., Dynamical model of the liquid-glass transition. *Phys. Rev. A* **29,** 2765 (1984).

Lewis, C. P., "Towards a Thermodynamic Understanding of the Glass Transition," Senior thesis, Dept. Chem. Eng., Princeton University, Princeton, NJ, 2000.

Liang, J., Edelsbrunner, H., Fu, P., Sudhakar, P. V., and Subramaniam, S., Analytical shape computation of macromolecules. I. Molecular area and volume through alpha shape. *Proteins* **33,** 1 (1998).

Lindemann, F. A., Über die berechnung molekularer eigenfrequenzen. *Phys. Z.* **11,** 609 (1910).

Lindsey, C. P., and Patterson, G. D., Detailed comparison of the William-Watts and Cole-Davidson functions. *J. Chem. Phys.* **73,** 3348 (1980).

Liu, C. Z.-W., and Oppenheim, I., Enhanced diffusion upon approaching the kinetic glass transition. *Phys. Rev. E* **53,** 799 (1996).

Lubachevsky, B. D., and Stillinger, F. H., Geometric properties of random disk packings. *J. Stat. Phys.* **60,** 561 (1990).

Lubachevsky, B. D., Stillinger, F. H., and Pinson, E. N., Disks vs. spheres: Contrasting properties of random packings. *J. Stat. Phys.* **64,** 501 (1991).

Mackenzie, J. D., Viscosity-temperature relationship for network liquids. *J. Am. Ceram. Soc.* **44,** 598 (1961).

Malandro, D. L., and Lacks, D. J., Volume dependence of potential energy landscapes in glasses. *J. Chem. Phys.* **107,** 5804 (1997).

Malandro, D. L., and Lacks, D. J., Molecular-level instabilities and enhanced self-diffusion in flowing liquids. *Phys. Rev. Lett.* **81,** 5576 (1998).

Malandro, D. L., and Lacks, D. J., Relationships of shear-induced changes in the potential energy landscape to the mechanical properties of ductile glasses. *J. Chem. Phys.* **110,** 4593 (1999).

Martin, C. J., and O'Connor, D. A., An experimental test of Lindemann's melting law. *J. Phys. C Sol. State Phys.* **10,** 3521 (1977).

Mel'cuk, A. I., Ramos, R. A., Gould, H., Klein, W., and Mountain, R. D., Long-lived structures in fragile glass-forming liquids. *Phys. Rev. Lett.* **75,** 2522 (1995).

Mishima, O., and Stanley, H. E., The relationship between liquid, supercooled and glassy water. *Nature* **396,** 329 (1998).

Moore, P., and Keyes, T., Normal mode analysis of liquid CS_2: Velocity correlation functions and self-diffusion constants. *J. Chem. Phys.* **100,** 6709 (1994).

Moynihan, C. T., Macedo, P. B., Montrose, C. J., Gupta, P. K., DeBolt, M. A., Dill, J. F., Dom, B. E., Drake, P. W., Easteal, A. J., Elterman, P. B., Moeller, R. P., Sasabe, H., and Wilder, J. A., *in* "The Glass Transition and the Nature of the Glassy State " (M. Goldstein and R. Simha, Eds.), *Ann. N.Y. Acad. Sci.* **279,** 15 (1976).

Ohmine, I., Liquid water dynamics: collective motions, fluctuation, and relaxation. *J. Phys. Chem.* **99,** 6767 (1995).

Ono, S., and Kondo, S., "Handbuch der Physik." Springer, Berlin, 1960, Vol. 10, p. 135.

Patashinski, A. Z., and Ratner, M. A., Inherent amorphous structures and statistical mechanics of melting. *J. Chem. Phys.* **106,** 7249 (1997).

Peng, D.-Y., and Robinson, D. B., A new two-constant equation of state. *Ind. Eng. Chem. Fundam.* **15,** 59 (1976).

Perera, D. N., and Harrowell, P., Measuring diffusion in supercooled liquids: The effect of kinetic inhomogeneities. *J. Chem. Phys.* **104,** 2369 (1996a).

Perera, D. N., and Harrowell, P., Consequence of kinetic inhomogeneities in glasses. *Phys. Rev. E* **54,** 1652 (1996b).

Phillips, W. A., Tunneling states in amorphous solids. *J. Low Temp. Phys.* **7,** 351 (1972).

Plazek, D. J., Bero, C. A., and Chay, I.-C., The recoverable compliance of amorphous materials. *J. Non-Cryst. Sol.* **172–174,** 181 (1994).

Plotkin, S. S., Wang, J., and Wolynes, P. G., Correlated energy landscape model for finite, random heteropolymers. *Phys. Rev. E* **53,** 6271 (1996).

Plotkin, S. S., Wang, J., and Wolynes, P. G., Statistical mechanics of a correlated energy landscape model for protein folding funnels. *J. Chem. Phys.* **106,** 2932 (1997).

Prausnitz, J. M., Molecular thermodynamics: Opportunities and responsibilities. *Fluid Phase Equil.* **116,** 12 (1996).

Rastogi, S., Höhne, G. W. H., and Keller, A., Unusual pressure-induced phase behavior in crystalline poly (4-methylpentene-1): Calorimetric and spectroscopic results and further implications. *Macromolecules* **32,** 8897 (1999).

Reid, R. C., Prausnitz, J. M., and Poling, B., "The Properties of Gases and Liquids," 4th ed., Appendix A, McGraw–Hill, New York, 1987.

Rein ten Wolde, P., Ruiz-Montero, M. J., and Frenkel, D., Numerical calculation of the rate of crystal nucleation in a Lennard-Jones system at moderate undercooling. *J. Chem. Phys.* **104,** 9932 (1996).

Reiss, H., Statistical geometry in the study of fluids and porous media. *J. Phys. Chem.* **96,** 4736 (1992).

Reiss, H., and Hammerich, A. D., Hard spheres—Scaled particle theory and exact relations on the existence and structure of the fluid-solid phase transition. *J. Phys. Chem.* **90,** 6252 (1986).

Richard, P., Oger, L., Troadec, J.-P., and Gervois, A., Geometrical characterization of hard-sphere systems. *Phys.-Rev. E* **60,** 4551 (1999).

Richert, R., Geometrical confinement and cooperativity in supercooled liquids studied by solvation dynamics. *Phys. Rev. B* **54,** 762 (1996).

Richert, R., and Angell, C. A., Dynamics of glass-forming liquids. V. On the link between molecular dynamics and configurational entropy. *J. Chem. Phys.* **108,** 9016 (1998).

Richert, R., and Blumen, A., Disordered systems and relaxation, *in* "Disorder Effects on Relaxational Processes" (R. Richert and A. Blumen, Eds.), p. 1. Springer, Berlin, 1994.

Rintoul, M. D., and Toquato, S., Algorithm to compute void statistics for random arrays of disks. *Phys. Rev. E* **52,** 2635 (1995).

Rintoul, M. D., and Torquato, S., Computer simulations of dense hard-sphere systems. *J. Chem. Phys.* **105,** 9258 (1996).

Roberts, C. J., Debenedetti, P. G., and Stillinger, F. H., Equation of state of the energy landscape of SPC/E water. *J. Phys. Chem. B* **103,** 10258 (1999).

Sahimi, M., Flow phenomena in rocks—From continuum models to fractals, percolation, cellular-automata, and simulated annealing. *Rev. Mod. Phys.* **65,** 1393 (1993).

Sahimi, M., "Flow and Transport in Media and Fractured Rock." VCH, Weinheim, Germany, 1995.

Sastry, S., Liquid limits: Glass transition and liquid-gas spinodal boundaries of metastable liquids. *Phys. Rev. Lett.* **85,** 590 (2000).

Sastry, S., Corti, D. S., Debenedetti, P. G., and Stillinger, F. H., Statistical geometry of particle packings. I. Algorithm for exact determination of connectivity, volume, and surface areas of void space in monodisperse and polydisperse sphere packings. *Phys. Rev. E* **56,** 5524 (1997a).

Sastry, S., Debenedetti, P. G., and Stillinger, F. H., Statistical geometry of particle packings. II. Weak spots in liquids. *Phys. Rev. E* **56,** 5533 (1997b).

Sastry, S., Debenedetti, P. G., and Stillinger, F. H., Signatures of distinct dynamical regimes in the energy landscape of a glass-forming liquid. *Nature* **393,** 554 (1998a).

Sastry, S., Truskett, T. M., Debenedetti, P. G., Torquato, S., and Stillinger, F. H., Free volume in the hard sphere liquid. *Mol. Phys.* **95,** 289 (1998b).

Saven, J. G., and Wolynes, P. G., Local signals in the entropy landscape of collapsed helical proteins. *Physica D* **107,** 330 (1997).

Saven, J. G., Wang, J., and Wolynes, P. G., Kinetics of protein folding: The dynamics of globally connected rough energy landscapes with biases. *J. Chem. Phys.* **101,** 11037 (1994).

Schulz, M., Energy landscape, minimum points, and non-Arrhenius behavior of supercooled liquids. *Phys. Rev. B* **57,** 11319 (1998).

Sciortino, F., Kob, W., and Tartaglia, P., Inherent structure entropy of supercooled liquids. *Phys. Rev. Lett.* **83,** 3214 (1999).

Shah, V. M., Stern, S. A., and Ludovice, P. J., Estimation of the free volume in polymers by means of a Monte Carlo technique. *Macromolecules* **22,** 4660 (1989).

Shahinpoor, M., Statistical mechanical considerations on the random packing of granular materials. *Powder Technol.* **25,** 163 (1980).

Shen, V. K., and Debenedetti, P. G., A computational study of homogeneous liquid-vapor nucleation in the Lennard–Jones fluid. *J. Chem. Phys.* **111,** 3581 (1999).

Simon, F., Über den zustand der unterkühlten flüssigkeiten und glässer. *Z. Anorg. Allg. Chem.* **203,** 219 (1931).

Sjögren, L., and Götze, W., α-Relaxation near the glass transition. *J. Non-Cryst. Sol.* **131–133,** 153 (1991).

Soave, G. S., Equilibrium constants from a modified Redlich–Kwong equation of state. *Chem. Eng. Sci.* **27,** 1197 (1972).

Speedy, R. J., Statistical geometry of hard-sphere systems. *J. Chem. Soc. Faraday Trans. II* **76,** 693 (1980).

Speedy, R. J., Relations between a liquid and its glasses. *J. Phys. Chem. B* **103,** 4060 (1999).

Steinhardt, P. J., Nelson, D. R., and Ronchetti, M., Bond-orientational order in liquids and glasses. *Phys. Rev. B* **28,** 784 (1983).

Stillinger, F. H., Role of potential energy scaling in the low-temperature relaxation behavior of amorphous materials. *Phys. Rev. B* **32,** 3134 (1985).

Stillinger, F. H., Supercooled liquids, glass transitions, and the Kauzmann paradox. *J. Chem. Phys.* **88,** 7818 (1988).

Stillinger, F. H., A topographic view of supercooled liquids and glass formation. *Science* **267,** 1935 (1995).

Stillinger, F. H., Enumeration of isobaric inherent structures for the fragile glass former o-terphenyl. *J. Phys. Chem. B* **102,** 2807 (1998).

Stillinger, F. H., Exponential multiplicity of inherent structures. *Phys. Rev. E* **59,** 48 (1999).

Stillinger, F. H., Inherent structures enumeration for low-density materials. *Phys. Rev. E,* **63,** 011110-1 (2001).

Stillinger, F. H., and Debenedetti, P. G., Distinguishing vibrational and structural equilibration contributions to thermal expansion. *J. Phys. Chem. B* **103,** 4052 (1999).

Stillinger, F. H., and Hodgdon, J. A., Translation-rotation paradox for diffusion in fragile glass-forming liquids. *Phys. Rev. E* **50,** 2064 (1994).

Stillinger, F. H., and Hodgdon, J. A., Reply to "Comment on 'Translation-rotation paradox for diffusion in fragile glass-forming liquids.'" *Phys. Rev. E* **53,** 2995 (1996).

Stillinger, F. H., and Stillinger, D. K., Negative thermal expansion in the Gaussian core model. *Physica A* **244,** 358 (1997).

Stillinger, F. H., and Weber, T. A., Hidden structure in liquids. *Phys. Rev. A* **25,** 978 (1982).

Stillinger, F. H., and Weber, T. A., Inherent structure-theory of liquids in the hard-sphere limit. *J. Chem. Phys.* **83,** 4767 (1985).

Stillinger, F. H., Debenedetti, P. G., and Sastry, S., Resolving vibrational and structural contributions to isothermal compressibility. *J. Chem. Phys.* **109,** 3983 (1998).

Takahara, S., Yamamuro, O., and Suga, H., Heat capacities and glass transitions of 1-propanol and 3-methylpentane under pressure. New evidence for the entropy theory. *J. Non-Cryst. Sol.* **171,** 259 (1994).

Tammann, G., and Hesse, W., Die abhängigkeit der viskosität von der temperature bei unterkühlten flüssigkeiten. *Z. Anorg. Allg. Chem.* **156,** 245 (1926).

Tanemura, M., Ogawa, T., and Ogita, N., A new algorithm for 3-dimensional Voronoi tessellation. *J. Comput. Phys.* **51,** 191 (1983).

Tarjus, G., and Kivelson, D., Breakdown of the Stokes–Einstein relation in supercooled liquids. *J. Chem. Phys.* **103,** 3071 (1995).

Theodorou, D. N., Symposium in print—Molecular modeling. *Chem. Eng. Sci.* **49,** 2715 (1994).

Thompson, K. E., and Fogler, H. S., Modeling flow in disordered packed beds from pore-scale fluid mechanics. *AIChE J.* **43,** 1377 (1997).

Torquato, S., Random heterogeneous media: Microstructure and improved bounds on effective properties. *Appl. Mech. Rev.* **44,** 37 (1991).

Torquato, S., Unified methodology to quantify the morphology and properties of inhomogeneous media. *Physica A* **207,** 79 (1994).

Torquato, S., Truskett, T. M., and Debenedetti, P. G., Is random close packing of spheres well defined? Phys. *Rev. Lett.* **84,** 2064 (2000).

Truskett, T. M., Torquato, S., and Debenedetti, P. G., Towards a quantification of disorder in materials: Distinguishing equilibrium and glassy sphere packings. *Phys. Rev. E* **62,** 993 (2000).

Uhlmann, D. R., A kinetic treatment of glass formation. *J. Non-Cryst. Sol.* **7,** 337 (1972).

Utz, M., Debenedetti, P. G., and Stillinger, F. H., Atomistic simulation of aging and rejuvenation in glasses. *Phys. Rev. Lett.* **84,** 1471 (2000).

Utz, M., Debenedetti, P. G., and Stillinger, F. H., Isotropic tensile strength of molecular glasses *J. Chem. Phys.* **114,** 10049 (2001).

van Duijneveldt, J. S., and Frenkel, D., Computer simulation study of free energy barriers in crystal nucleation. *J. Chem. Phys.* **96,** 4655 (1992).

Vidal Russell, E., and Israeloff, N. E., Direct observation of molecular cooperativity near the glass transition. *Nature* **408,** 695 (2000).

Vishnyakov, A., Debenedetti, P. G., and Neimark, A. V., Statistical geometry of cavities in a metastable confined fluid. *Phys. Rev. E* **62,** 538 (2000).

Vogel, H., Das temperatur-abhängigkeitsgesetz der viskosität von flüssigkeiten. *Phys. Zeit.* **22,** 645 (1921).

Wang, C.-Y., and Ediger, M. D., How long do regions of different dynamics persist in supercooled o-terphenyl? *J. Phys. Chem. B* **103,** 4177 (1999).

Wang, J., Onuchic, J., and Wolynes, P., Statistics of kinetic pathways on biased rough energy landscapes with applications to protein folding. *Phys. Rev. Lett.* **76,** 4861 (1996).

Weber, T. A., and Stillinger, F. H., Inherent structures and distribution-functions for liquids that freeze into bcc crystals. *J. Chem. Phys.* **81,** 5089 (1984).

Weber, T. A., and Stillinger, F. H., Interactions, local order, and atomic rearrangement kinetics in amorphous nickel-phosphorus alloys. *Phys. Rev. B* **32,** 5402 (1985).

Weber, T. A., Fredrickson, G. H., and Stillinger, F. H., Relaxation behavior in a tiling model for glasses. *Phys. Rev. B* **34,** 7641 (1986).

Wilks, J., "The Properties of Liquid and Solid Helium." Clarendon Press, Oxford, 1967.

Williams, G., and Watts, D. C., Non-symmetrical dielectric relaxation behavior arising from a simple empirical decay function. *Trans. Faraday Soc.* **66,** 80 (1970).

Wolynes, P. G., Aperiodic crystals: Biology, chemistry and physics in a fugue with stretto, *in* "Proceedings of the International Symposium on Frontiers in Science" (S. S. Chan and P. G. Debrunner, Eds.), *AIP Conf. Proc.* **180,** 39 (1988).

Wolynes, P. G., Randomness and complexity in chemical physics. *Acc. Chem. Res.* **25,** 513 (1992).

Wolynes, P. G., Entropy crises in glasses and random heteropolymers. *J. Res. Natl. Inst. Stand. Tech.* **102,** 187 (1997).

Wolynes, P. G., Onuchic, J. N., and Thirumalai, D., Navigating the folding routes. *Science* **267,** 1619 (1995).

Wu, T., and Tsay, S., Instantaneous normal mode analysis of liquid Na. *J. Chem. Phys.* **105,** 9281 (1996).

Zallen, R., "The Physics of Amorphous Solids." Wiley, New York, 1983.

Zarzycki, J., "Glasses and the Vitreous State." Cambridge University Press, Cambridge, 1991.

Ziman, J. M., "Models of Disorder. The Theoretical Physics of Homogeneously Disordered Systems," Cambridge University Press, Cambridge, 1979.